© 2017. Published by The Company of Biologists Ltd | Journal of Cell Science (2017) 130, 2382-2393 doi:10.1242/jcs.197434

RESEARCH ARTICLE

ARHGAP42 is activated by Src-mediated tyrosine phosphorylation to promote cell motility

Weifeng Luo[3,‡], Radoslav Janoštiak[1,‡], Ondřej Tolde[1,2,‡], Larisa M. Ryzhova[3,*,‡], Lenka Koudelková[1,2], Michal Dibus[1,2], Jan Brábek[1,2], Steven K. Hanks[3] and Daniel Rosel[1,2,§]

ABSTRACT

The tyrosine kinase Src acts as a key regulator of cell motility by phosphorylating multiple protein substrates that control cytoskeletal and adhesion dynamics. In an earlier phosphotyrosine proteomics study, we identified a novel Rho-GTPase activating protein, now known as ARHGAP42, as a likely biologically relevant Src substrate. ARHGAP42 is a member of a family of RhoGAPs distinguished by tandem BAR-PH domains lying N-terminal to the GAP domain. Like other family members, ARHGAP42 acts preferentially as a GAP for RhoA. We show that Src principally phosphorylates ARHGAP42 on tyrosine 376 (Tyr-376) in the short linker between the BAR-PH and GAP domains. The expression of ARHGAP42 variants in mammalian cells was used to elucidate its regulation. We found that the BAR domain is inhibitory toward the GAP activity of ARHGAP42, such that BAR domain deletion resulted in decreased active GTP-bound RhoA and increased cell motility. With the BAR domain intact, ARHGAP42 GAP activity could be activated by phosphorylation of Tyr-376 to promote motile cell behavior. Thus, phosphorylation of ARHGAP42 Tyr-376 is revealed as a novel regulatory event by which Src can affect actin dynamics through RhoA inhibition.

KEY WORDS: Src, Motility, RhoA, GAP, GRAF, Focal adhesion, Tyrosine phosphorylation

INTRODUCTION

Src is a nonreceptor protein tyrosine kinase that becomes activated following the engagement of many different classes of cellular receptors, including receptor protein tyrosine kinases, integrins and other adhesion receptors, and cytokine and G protein-coupled receptors, and thereby participates in signaling pathways that control cell cycle progression, apoptosis, cell adhesion and migration (reviewed in Frame, 2004). Deregulation of Src activity by overexpression or mutation can result in oncogenic cell transformation and invasive properties. Elevated Src activity is commonly observed in tumors and Src has become an established therapeutic target (reviewed in Rosel et al., 2013).

[1]Department of Cell Biology, Charles University in Prague, Viničná 7, Prague, 12843, Czech Republic. [2]Department of Cell Biology, Biotechnology and Biomedicine Centre of the Academy of Sciences and Charles University (BIOCEV), Průmyslová 595, Vestec u Prahy 25242, Czech Republic. [3]Department of Cell and Developmental Biology, Vanderbilt University School of Medicine, Nashville, TN 37232, USA.
*Present address: Center for Molecular Medicine, Maine Medical Center Research Institute, Scarborough, ME 04074, USA.
‡These authors contributed equally to this work

§Author for correspondence (rosel@natur.cuni.cz)

D.R., 0000-0001-7221-8672

Received 13 September 2016; Accepted 26 May 2017

Src plays an essential role in cell migration through regulation of cytoskeletal organization and adhesion dynamics. 'SYF' fibroblasts (from mice lacking the Src-family kinases Src, Yes and Fyn) or fibroblasts ectopically expressing kinase-inactive Src exhibit impaired migration and large peripheral adhesions with reduced turnover (Fincham and Frame, 1998; Klinghoffer et al., 1999). In agreement, elevated Src activity is associated with the disruption of actin stress fibers followed by disassembly of focal adhesions (Fincham et al., 1999; Frame et al., 2002; Webb et al., 2004).

Src can regulate focal adhesion dynamics through distinct pathways. A well-studied pathway involves focal adhesion kinase (FAK, also known as PTK2) (reviewed in Hanks et al., 2003). Upon integrin receptor activation, FAK autophosphorylates tyrosine 397 to create a binding site for the Src SH2 domain, resulting in Src recruitment to nascent focal adhesions. FAK phosphorylation at tyrosine 925 by Src results in activation of Erk proteins via the Grb2/SOS/Ras pathway (Schlaepfer et al., 1994) and subsequently the activation of MLCK (also known as MYLK), which is important for actin dynamics at lamellipodia (Cheresh et al., 1999). The FAK–Src complex phosphorylates p130Cas and paxillin (Hanks et al., 2003; Nojima et al., 1995), resulting in recruitment of the Rac-specific GEFs DOCK180 and β-PIX to focal adhesions (Kiyokawa et al., 1998; ten Klooster et al., 2006). Elevated activity of Rac promotes membrane ruffling, lamellipodium formation, and further formation of nascent focal adhesions by acting on the WASP and WAVE (also known as WAS and WASF) family of Arp2/3 complex activators to stimulate actin polymerization (Eden et al., 2002; Klemke et al., 1998; Miki et al., 2000; Welch and Mullins, 2002). Src can also affect cytoskeletal organization by direct regulation of the activity of Rho GTPases. For example, the FAK–Src complex downregulates RhoA activity through Src-mediated tyrosine phosphorylation of p190RhoGAP (also known as ARHGAP35), thereby elevating its RhoGAP activity (Arthur et al., 2000; Bass et al., 2008). Downregulation of RhoA leads to upregulation of Rac, which in turn results in increased lamellipodial activity and focal adhesion dynamics (Huveneers and Danen, 2009; Ren et al., 2000).

Although many Src substrates have been identified, there is still much to learn about the multiple roles of Src in regulating cell behavior and transformation. Previously, we employed a proteomics approach to acquire a global view of the impact of oncogenic Src on the phosphotyrosine proteome of mouse embryonic fibroblasts (Luo et al., 2008). Among the novel putative Src substrates identified in that study was a then uncharacterized protein annotated as 'similar to oligophrenin-1'. The 'similar to oligophrenin-1' protein has subsequently been described as 'Rho GTPase-activating protein 42', encoded by the mouse gene *Arhgap42* (UniProtKB/Swiss-Prot accession number B2RQE8), and is a fourth mammalian member of a family of RhoGAPs that have N-terminal tandem Bin/amphiphysin/Rvs (BAR) and pleckstrin homology (PH) domains. In the present study, we have further characterized this protein

Journal of Cell Science

Journal of Cell Science (2017) 130, 2382-2393 doi:10.1242/jcs.197434

(herein designated as ARHGAP42) in order to gain insight into its cellular function and regulation. We show that ARHGAP42 localizes to stress fibers and focal adhesions, and possesses GAP activity towards RhoA, which is autoinhibited by its BAR domain. Moreover, we show that Src-mediated phosphorylation of ARHGAP42 tyrosine 376 (Tyr-376) stimulates GAP activity to promote focal adhesion dynamics and cell motility.

RESULTS

The putative Src substrate ARHGAP42, a member of the BAR-PH RhoGAP family, associates with focal adhesions and actin stress fibers

To study ARHGAP42, we isolated a cDNA that encodes a full-length mouse protein of 875 amino acid residues (98.6 kDa). Mouse ARHGAP42 is highly similar throughout its length to human ARHGAP42 (Fig. S1). We noted that mouse ARHGAP42 encoded by our full-length cDNA is 34 residues longer than the predicted mouse ARHGAP42 from UniProtKB (accession number B2RQE8), due to the predicted mouse ARHGAP42 missing part of the BAR domain. We also obtained cDNAs encoding a variant of mouse ARHGAP42 that lacks the same 34 residues in the BAR domain, indicating that this may be a naturally occurring splice variant. In the present study, we examined mouse ARHGAP42 that contains the full BAR domain.

ARHGAP42 belongs to a RhoGAP family characterized by N-terminal tandem BAR and PH domains, followed by a central GAP domain (Fig. 1A). The other mammalian members of this BAR-PH RhoGAP family are oligophrenin-1, encoded by a gene mutated in X-linked mental retardation (Billuart et al., 1998), GTPase regulator associated with FAK (GRAF; also known as ARHGAP26) (Hildebrand et al., 1996), and PH and SH3 domain-containing RhoGAP protein (PSGAP; also known as GRAF2 or ARHGAP10) (Ren et al., 2001; Shibata et al., 2001). ARHGAP42 has alternatively been referred to as 'GRAF3' (Bai et al., 2013). Genes encoding BAR-PH RhoGAPs are also present in *Drosophila* (gene CG8948, encoding Dm Graf) and *C. elegans* (gene T04C9.1). ARHGAP42 contains a C-terminal SH3 domain, a feature common to all known BAR-PH family members with the exception of oligophrenin-1. However, if the SH3 domain is excluded, ARHGAP42 is overall most closely related to oligophrenin-1 (Fig. 1B). The mouse ARHGAP42 tyrosine residue corresponding to the phosphorylated tyrosine (pTyr) site identified in our phosphoproteomics study (Luo et al., 2008) is Tyr-376, which lies in the short linker region between the PH and GAP domains. This tyrosine residue is conserved in oligophrenin-1 and GRAF, but not in PSGAP. An *in vitro* assay of the isolated ARHGAP42 GAP domain demonstrated GAP activity toward RhoA and Cdc42, but not Rac1 (Fig. 1C), similar to the specificities reported for other members of the BAR-PH RhoGAP family (Billuart et al., 1998; Hildebrand et al., 1996; Ren et al., 2001).

To gain insight into cellular function, the subcellular localization of ARHGAP42 was examined. A GFP-tagged variant of ARHGAP42 was expressed in MEFs and cells were fixed and analyzed by fluorescence microscopy. Interestingly, GFP-ARHGAP42 localized prominently to both focal adhesions and actin stress fibers (Fig. 1D,E; Fig. S2). Further analysis indicated that the SH3 domain was indispensable for ARHGAP42 targeting to both actin stress fibers and focal adhesions (Fig. S2). These findings suggest a possible role for ARHGAP42 as a regulator of cell adhesion and actin cytoskeletal dynamics.

Src phosphorylates ARHGAP42 Tyr-376

In our phosphoproteomics study, ARHGAP42 pTyr-376 was readily detected in both Src-transformed mouse embryonic fibroblasts (MEFs) and counterpart nontransformed cells, a property indicative of biologically relevant Src substrates (Luo et al., 2008). The ability of Src to phosphorylate ARHGAP42 was further investigated; first using a COS-7 cell coexpression assay. To evaluate Tyr-376 as a site of phosphorylation, a variant of ARHGAP42 with Tyr-376 changed to phenylalanine (Y376F) was prepared. Wild-type (WT) or Y376F ARHGAP42 variants with an N-terminal GFP tag were expressed either alone or together with constitutively active mouse Src (Src-F529), after which ARHGAP42 tyrosine phosphorylation was assessed by immunoprecipitation with anti-GFP antibody and immunoblotting with either an anti-pTyr antibody or a phosphospecific antibody (pY376) directed against the phosphorylated Tyr-376 site. In COS-7 cells, GFP-ARHGAP42 expressed as a major band of expected size (~130 kDa) as well as a minor band that could be a degradation product. Src-F529 coexpression resulted in greatly elevated WT GFP-ARHGAP42 tyrosine phosphorylation, as detected by both pTyr and pY376 antibodies (Fig. 2A). By contrast, the Y376F variant was very poorly recognized by the pY376 antibody and recognition by the anti-pTyr antibody was much reduced in comparison to the WT (Fig. 2A, top panel; note the higher level of total Y376F versus WT in lanes 6 and 4, respectively). In a similar set of experiments carried out in MEFs, enhanced tyrosine phosphorylation of WT GFP-ARHGAP42 resulting from Src-F529 coexpression was again evident, and further shown to be sensitive to the Src inhibitor saracatinib (Fig. 2B). The ability of Src-F529 to directly phosphorylate ARHGAP42 Tyr-376 was further demonstrated by *in vitro* kinase assays of immunoprecipitates (Fig. 2C). Thus, Tyr-376 appears to be the major site of ARHGAP42 phosphorylation by Src.

The BAR and GAP domains of ARHGAP42 have mutually inhibitory properties

To further study ARHGAP42 function and regulation, GFP-tagged ARHGAP42 variants lacking either the BAR (ΔBAR), or GAP (ΔGAP) domains were expressed in MEFs. Immunoblot analysis using an antibody raised against ARHGAP42 showed that the variants were expressed to similar levels and gave rise to protein bands of expected sizes (Fig. 3A). When further assessing expression using fluorescence microscopy, it was apparent that the ΔBAR variant, in particular, caused a large fraction of the cells to take on an unusual dendritic-like arborized morphology characterized by a rounded cell body and numerous thin beaded extensions (Fig. 3B). In quantitative analysis, 56% of cells expressing GFP-ARHGAP42-ΔBAR were scored as having this arborized morphology, while only 8% of cells expressing GFP-ARHGAP42-WT took on this morphology (Fig. 3C). Such arborized cell morphology is characteristically observed when the RhoA/ROCK pathway is inhibited by various means (Omelchenko et al., 2002; Tatsis et al., 1998), including overexpression of different RhoGAP proteins such as p190RhoGAP or ARHGAP6 (Jiang et al., 2008; Prakash et al., 2000). Indeed, GFP-ARHGAP42-ΔGAP, which lacks the ability to inhibit RhoA, was unable to arborize cells (Fig. 3C). These observations suggest that the BAR domain of ARHGAP42 is autoinhibitory toward the GAP domain, such that GAP activity is elevated when the BAR domain is deleted. In a separate experiment, RhoA-GTP levels were assessed in MEFs stably expressing either ARHGAP42-WT or ARHGAP42-ΔBAR and, as predicted, RhoA-GTP levels were found to be significantly

Journal of Cell Science (2017) 130, 2382-2393 doi:10.1242/jcs.197434

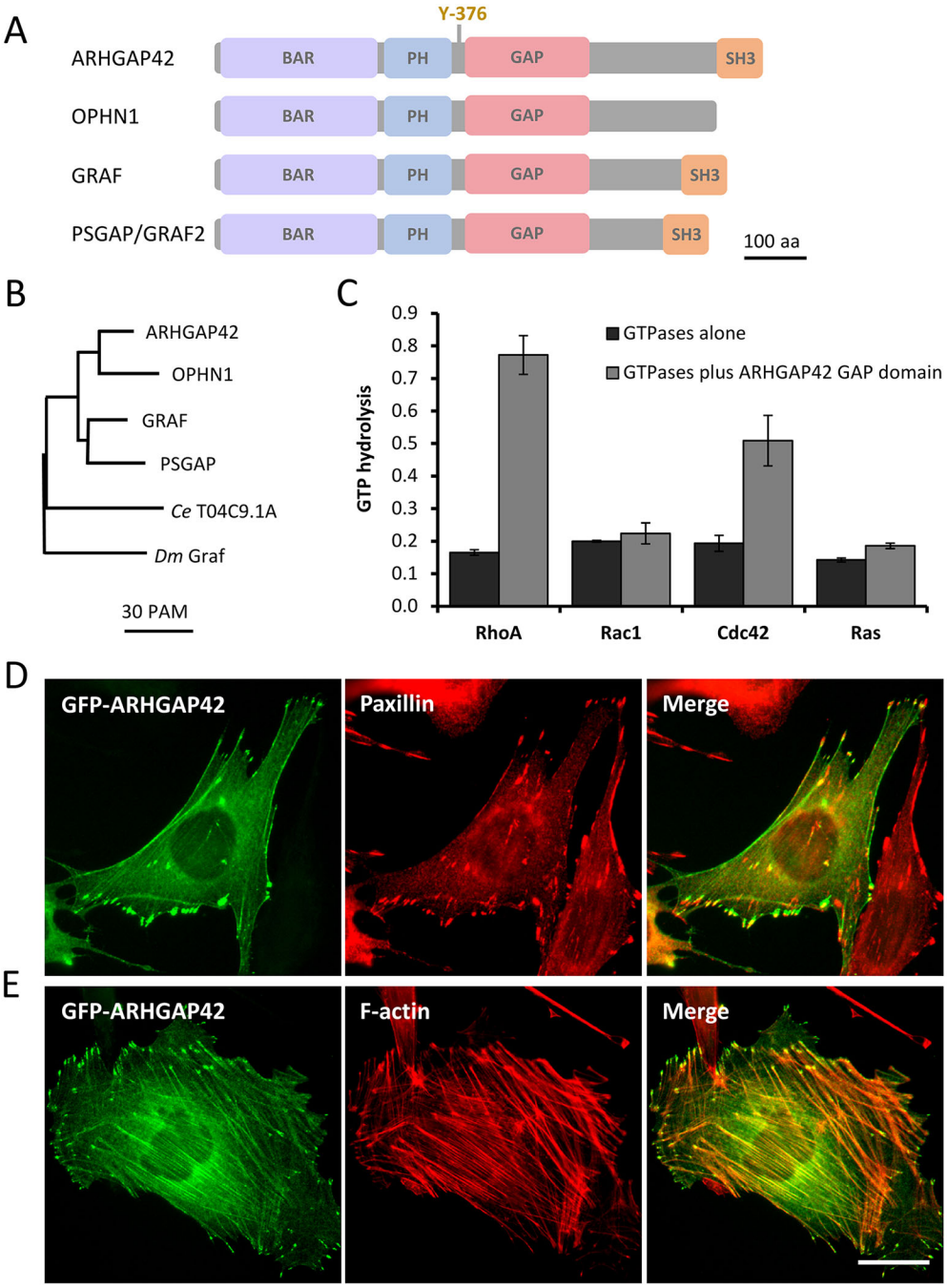

Fig. 1. Domain organization, phylogeny, substrate specificity and subcellular localization of ARHGAP42. (A) Domain organization of ARHGAP42 in comparison to the three other mammalian members of the BAR-PH RhoGAP family. For ARHGAP42, the position of the major site of Src-mediated phosphorylation, Tyr-376, is indicated. OPHN1, oligophrenin-1. (B) Phylogram showing evolutionary relationships among the mammalian BAR-PH RhoGAP family members and to more distant relatives predicted from *C. elegans* (*Ce* T04C9.1A) and *Drosophila* (*Dm* Graf) genomes. The phylogram was generated using Multalin software (Corpet, 1988). (C) ARHGAP42 is a GAP for RhoA and Cdc42, but not Rac1. The GAP domain of ARHGAP42 was bacterially expressed, recovered as a GST fusion protein, and assessed for its activity toward the Rho GTPases RhoA, Rac1 and Cdc42 by measuring the amount of phosphate released by GTP hydrolysis using an *in vitro* assay. Ras was included as a negative control. Values are mean±s.d. from triplicate assays. (D,E) MEFs were transfected with GFP-ARHGAP42 expression plasmid and viewed 24 h later by fluorescence microscopy of fixed cells. The cells were either immunostained with an antibody against paxillin to mark focal adhesions (D, red) or with phalloidin to mark F-actin (E, red). In the representative cell shown in D, GFP-ARHGAP42 is most prominently localized at the focal adhesions and actin stress fibers. In the representative cell shown in E, GFP-ARHGAP42 is more prominently observed in association with actin stress fibers, as well as in apparent focal adhesions. Scale bar: 30 µm.

lower in cells expressing the ΔBAR variant (Fig. 3D), indicative of elevated RhoGAP activity.

Tandem N-terminal BAR and PH domains are found not only in the members of the BAR-PH RhoGAP family but also in other proteins, including APPL1, APPL2 and centaurin α2 (also known as ADAP2), indicating that this organization has been evolutionarily conserved as a functional unit. Structural and biochemical studies have shown the BAR-PH module to form elongated crescent-shaped dimers that function in the sensing and induction of membrane curvature (Li et al., 2007; Peter et al., 2004; Zhu et al., 2007). The ability of the BAR-PH module to induce plasma membrane curvature can be observed as tubulovesicular membrane structures when expressed in cells (Lundmark et al., 2008; Peter et al., 2004). We employed this membrane tubulation assay to further examine the function and regulation of ARHGAP42. GFP-ARHGAP42-WT and -ΔGAP variants (and vector only control) were expressed in COS-7 cells (Fig. 4A) and analyzed 48 h later for membrane tubulation by fluorescence microscopy. The striking tubulovesicular membranes were apparent in many cells expressing GFP-ARHGAP42-WT and -ΔGAP (Fig. 4B,C), but were not observed in the vector only control cells. Notably, tubulovesicular membranes were observed in a significantly higher fraction of cells expressing GFP-ARHGAP42-ΔGAP (84%) as compared to cells expressing GFP-ARHGAP42-WT (27%) (Fig. 4C), even though the WT protein was expressed to a higher level. The finding that deletion of the ARHGAP42 GAP domain results in enhanced tubulovesicular membrane formation indicates that the GAP domain is also autoinhibitory to the BAR-PH module.

Journal of Cell Science (2017) 130, 2382-2393 doi:10.1242/jcs.197434

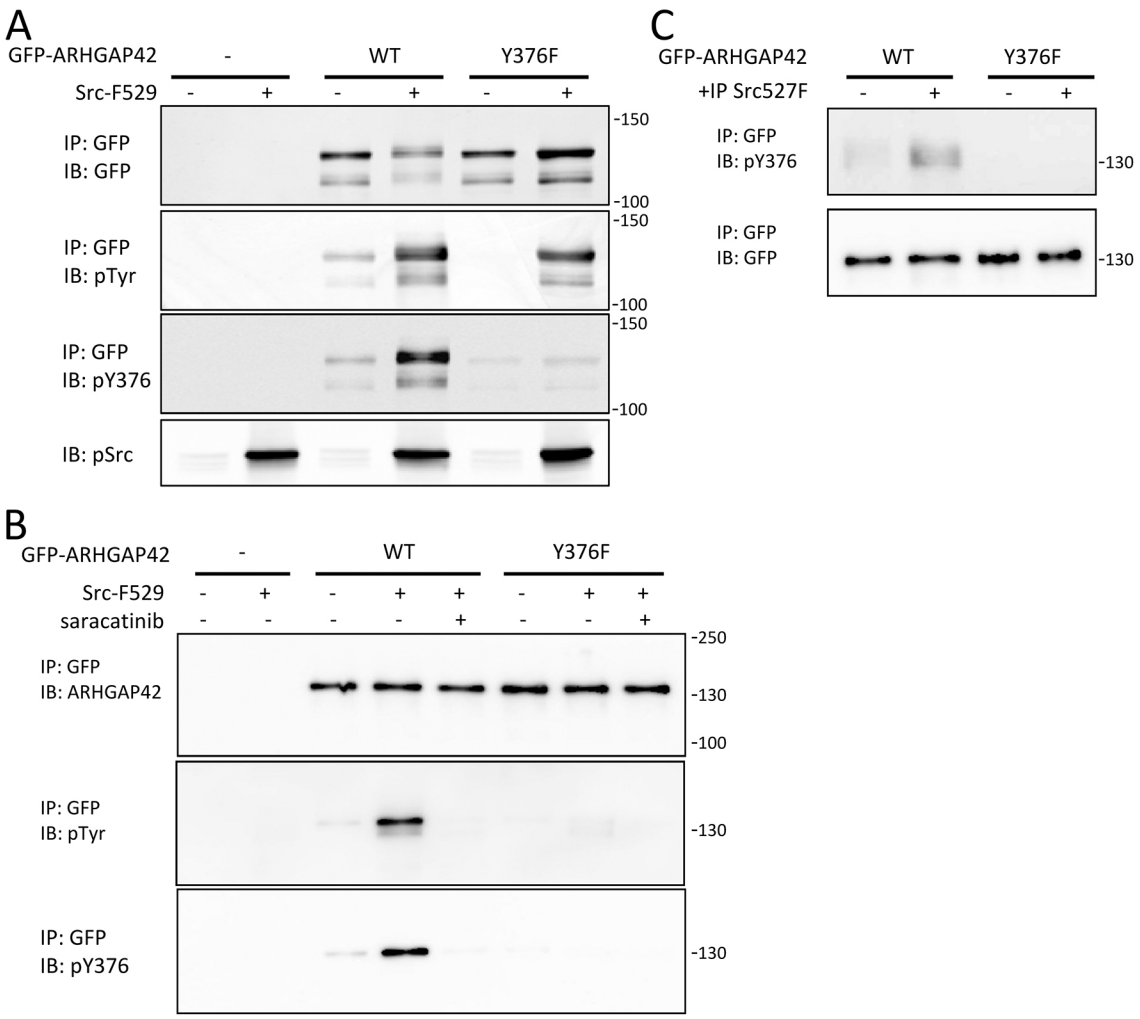

Fig. 2. Src promotes phosphorylation of ARHGAP42 Tyr-376. (A,B) Immunoblot analysis of GFP-ARHGAP42 phosphorylation. GFP-ARHGAP42 variants were transiently expressed in (A) COS-7 cells or (B) MEFs, either with or without constitutively active Src-F529, and ARHGAP42 tyrosine phosphorylation was assessed by immunoprecipitation (IP) with anti-GFP antibody followed by immunoblotting (IB) with general anti-pTyr (pTyr) or anti-pTyr376 (pY376) antibody. (B) Prior to immunoprecipitation in MEFs, Src activity was further manipulated by incubating the cells for 2 h in the presence or absence of 5 µM saracatinib. Src-F529 expression was confirmed by immunoblot analysis of total cell lysates with antibody against the Src autophosphorylation site (pSrc). (C) *In vitro* kinase assay. GFP-ARHGAP42 variants were individually expressed in MEFs and immunoprecipitated using anti-GFP antibody, eluted, and incubated with immunoprecipitated Src-F529. After the kinase reaction had been carried out for 1.5 h, levels of GFP-ARHGAP42 phosphorylation were assessed using a pY376 antibody. The numbers on the right indicate the positions of molecular size markers (kDa).

ARHGAP42-ΔBAR promotes focal adhesion dynamics and cell migration

Because RhoA is a known regulator of focal adhesion dynamics and cell migration (Lessey et al., 2012; Raftopoulou and Hall, 2004), it was of interest to further study ARHGAP42 by assessing these cellular properties in MEFs stably expressing either GFP-ARHGAP42-WT, GFP-ARHGAP42-ΔBAR or GFP-ARHGAP42-ΔGAP. Confocal immunofluorescence microscopy revealed that focal adhesion size is decreased in cells expressing GFP-ARHGAP42-ΔBAR as compared to cells expressing GFP-ARHGAP42-WT, whereas cells expressing the ΔGAP variant have significantly larger focal adhesions (Fig. 5A; Fig. S3A). Increased focal adhesion size could be caused by decreased focal adhesion turnover. To assess focal adhesion dynamics, the focal adhesion marker mCherry-zyxin was expressed in MEFs expressing ARHGAP42 variants and confocal live-cell microscopy was used to determine the percentage of adhesions that either assembled or disassembled during a 20 min time interval. As anticipated, the focal adhesion dynamics was highest in cells expressing the ΔBAR variant of ARHGAP42 and lowest in cells expressing the ΔGAP variant (Fig. 5B). To strengthen the observation of the effect of the ARHGAP42 variants on focal adhesion dynamics, we further investigated the exchange dynamics of vinculin within focal adhesions using fluorescence recovery after photobleaching (FRAP) experiments. Consistent with the above results, vinculin dynamics in focal adhesions was highest (slowest half-maximum recovery) in cells expressing the ΔBAR variant of ARHGAP42 and lowest in cells expressing the ΔGAP variant (Fig. 5C; Fig. S3B). Because adhesion dynamics are tightly interconnected with 2D cell migration (Kim and Wirtz, 2013; Webb et al., 2004), the influence of the ARHGAP42 variants on monolayer wound healing was assessed. Consistent with the results on focal adhesion size and turnover, MEFs expressing the ΔBAR variant healed the wounded area significantly faster than the cells expressing the other ARHGAP42 variants (Fig. 5D; Fig. S3C). Taken together, these data indicate that the elevated GAP activity of the ARHGAP42-

Journal of Cell Science (2017) 130, 2382-2393 doi:10.1242/jcs.197434

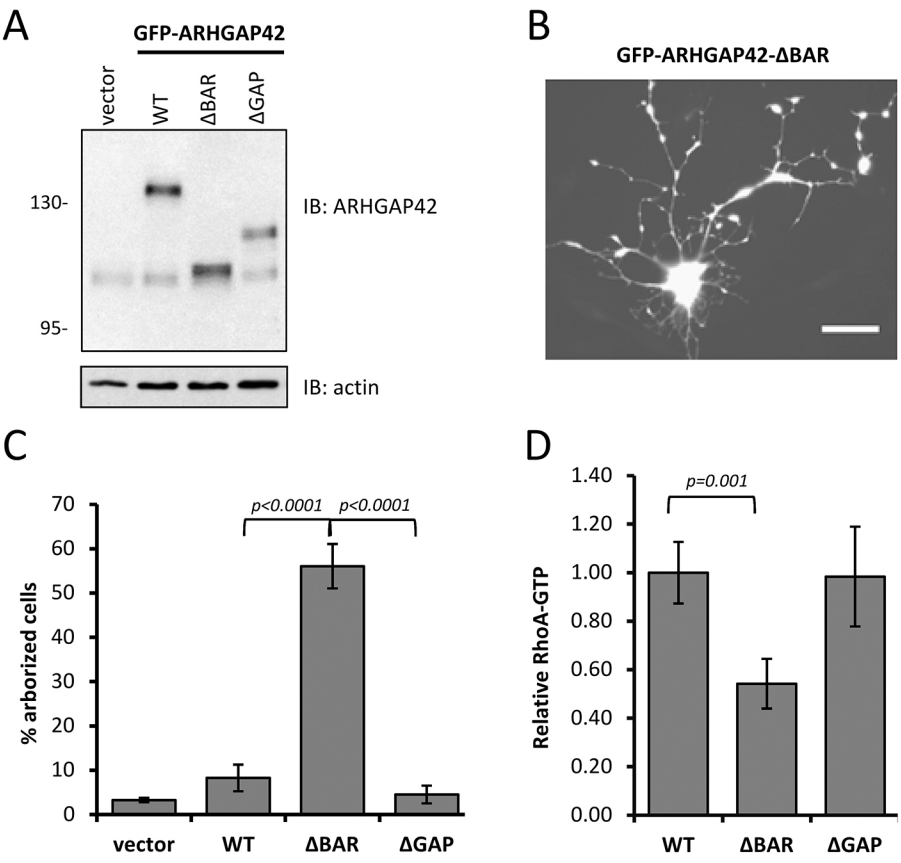

Fig. 3. ARHGAP42 with deleted BAR domain has enhanced RhoGAP activity. (A) MEFs were transfected with plasmids expressing GFP-ARHGAP42 variants WT, ΔBAR or ΔGAP, and 24 h later the cell lysates were analyzed by immunoblotting with an antibody raised against mouse ARHGAP42. The ARHGAP42 antibody detects the GFP-tagged variants as well as an additional band of expected size for the endogenous protein. Actin was detected as an additional loading control (bottom panel). The numbers indicate the positions of molecular size markers (kDa). (B) Example of a highly arborized MEF cell expressing GFP-ARHGAP42-ΔBAR. 24 h after transfection, the cell was fixed and visualized for GFP fluorescence. Scale bar: 30 µm. (C) Quantification of arborized morphology in MEFs expressing GFP-ARHGAP42 variants. Values are mean±s.d. from four independent transfections, with 500 fluorescent cells scored per transfection. (D) Deletion of the BAR domain significantly enhances the RhoGAP activity of ARHGAP42. Lysates from MEFs stably expressing ARHGAP42 variants were analyzed using a G-LISA assay to detect GTP-bound RhoA. Values are mean±s.d. RhoGTP signal compared to the signal from ARHGAP42-WT cells from three independent experiments. *P*-values indicate statistical significance determined by one-way ANOVA followed by Tukey's multiple comparisons test.

ΔBAR variant gives rise to enhanced focal adhesion dynamics and cell migration.

ARHGAP42 is activated by Src – requirement for the Tyr-376 phosphorylation site

The experiments described above showed that the GAP domain of ARHGAP42 can be activated by deletion of the BAR domain, and that GAP activity can be measured as changes in cell shape and dynamics. Similar approaches were undertaken to investigate the regulatory role of ARHGAP42 Tyr-376 phosphorylation. In initial experiments, either GFP-ARHGAP42-WT or GFP-ARHGAP42-Y376F was transiently expressed in v-Src-transformed versus nontransformed NIH-3T3 fibroblasts. Anti-pTyr antibody readily recognized GFP-ARHGAP42-WT expressed in the v-Src-transformed cells, but not GFP-ARHGAP42-Y376F (Fig. 6A). In the nontransformed cells, both WT and Y376F variants localized to stress fibers (Fig. 6C, left two panels). However, detailed analysis of its enrichment in longitudinal section through focal adhesions showed that GFP ARHGAP42 Y376F is mostly absent from the front side of the focal adhesions (Fig. S2B,D). Expression of the ARHGAP42 variants in the v-Src-transformed cells had a different outcome. When GFP-ARHGAP42-WT was expressed in v-Src-NIH-3T3, almost all cells (95%) took on the rounded arborized morphology (Fig. 6B,C), indicating that the GAP activity of ARHGAP42 was highly elevated in the presence of v-Src. In vector control cells expressing GFP only, 16% of the v-Src-transformed cells were scored as being rounded or arborized; a background value reflective of the classical v-Src-mediated fusiform morphology. Most notably, GFP-ARHGAP42-Y376F was unable to promote arborization in v-Src-NIH-3T3 cells above this background level (Fig. 6B). GFP-ARHGAP42-Y376F was observed to associate with structures reminiscent of podosome rosettes in in v-Src-NIH-3T3 cells (Fig. 6C, rightmost panel). These results indicate that Src-mediated phosphorylation of ARHGAP42 Tyr-376 acts as a mechanism to promote the GAP activity of ARHGAP42, resulting in RhoA inhibition and the arborized phenotype.

The effect of Src-mediated phosphorylation of ARHGAP42 Tyr-376 on RhoA activity was also analyzed in SYF cells, which are triple nulls for Src, Yes and Fyn, and thus lacking in endogenous Src-family kinase activity (Klinghoffer et al., 1999). Indeed, we found that RhoA-GTP levels are significantly lower in SYF cells stably expressing ARHGAP42-WT as compared to ARHGAP42-Y376F, but only when Src activity in the SYF cells was restored by expression of Src-F529 (Fig. 7A,B). To strengthen our observations that ARHGAP42 affects RhoA activity in a Tyr-376 phosphorylation-dependent manner, we performed a pull-down analysis with a bacterially expressed constitutively active form of RhoA (RhoA-CA), as described in García-Mata et al. (2006). We found that the ability of RhoA-CA to pull down ARHGAP42-WT, but not ARHGAP42-Y376F, is greatly enhanced in SYF cells expressing Src-F529 (Fig. 7C,D). This agrees with the decreased levels of RhoA-GTP in SYF+Src-F529 cells expressing GFP-ARHGAP42-WT, and strongly indicates that its GAP activity is responsible for the decrease.

The SYF cells were further employed to investigate the impact of Src-mediated phosphorylation of ARHGAP42 Tyr-376 on the regulation of focal adhesion dynamics and migration. Initially, focal adhesion size was analyzed in SYF versus SYF+Src-F529 cells transfected with GFP-ARHGAP42 variants. Analysis by confocal fluorescence microscopy revealed that the presence of Src activity (Src-F529) leads to decreased focal adhesion size in cells expressing

Journal of Cell Science (2017) 130, 2382-2393 doi:10.1242/jcs.197434

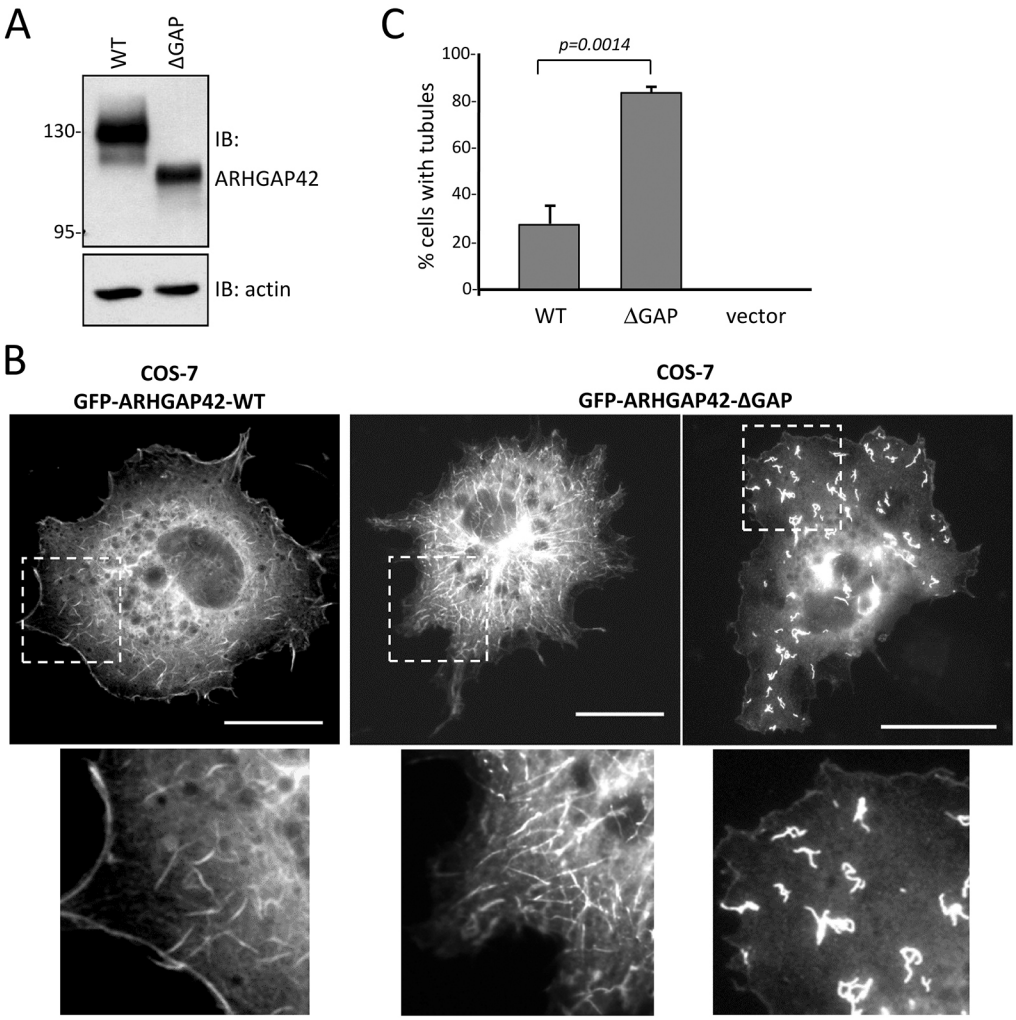

Fig. 4. Expression of ARHGAP42 promotes membrane tubulation that is enhanced by deletion of the GAP domain. Plasmids expressing GFP-ARHGAP42-WT versus -ΔGAP (or the empty vector) were transfected into COS-7 cells and the cells were analyzed 48 h later. (A) Immunoblot analysis of whole cell lysates shows expression levels of the ARHGAP42 variants, with actin as a control for equal loading. (B) Representative cells expressing GFP-ARHGAP42-WT (left) and GFP-ARHGAP42-ΔGAP (middle and right, exhibiting membrane tabulation). The cells were fixed and visualized for GFP fluorescence. The boxed regions in the upper panels are enlarged in the lower panels. Scale bars: 30 µm. (C) Quantitative analysis of membrane tubulation induced by ARHGAP42 variants. Values are mean±s.d. from four independent transfection experiments, with 500 cells scored per experiment. Statistical significance was determined by one-way ANOVA followed by Tukey's multiple comparisons test.

ARHGAP42-WT, but not in cells expressing ARHGAP42-Y376F (Fig. 8A). Expression of ARHGAP42-ΔBAR also gave rise to decreased focal adhesion size, but unlike ARHGAP42-WT, this was observed in both SYF and SYF+Src-F529 cells (Fig. 8A). These results indicate that Src-mediated phosphorylation of ARHGAP42 Tyr-376 results in activation of the GAP activity of ARHGAP42, similar to what is achieved by deletion of the BAR domain. The effect of ARHGAP42 GAP activity on focal adhesion dynamics was then assessed in these cells. Live-cell microscopy showed that Src activity resulted in increased focal adhesion dynamics in cells expressing ARHGAP42-WT and ARHGAP42-ΔBAR, but this was not the case for cells expressing ARHGAP42-Y376F (Fig. 8B; Fig. S4A). RhoA inhibition can lead to upregulation of Rac to stimulate lamellipodial dynamics (Cheresh et al., 1999; Ridley et al., 1992; Rottner et al., 1999; Sharma and Mayer, 2008). Therefore, we also analyzed the velocity of lamellipodial protrusions in SYF and SYF+SrcF cells expressing the ARHGAP42 variants. Kymograph analysis showed that the presence of Src activity in SYF+SrcF cells expressing ARHGAP42-WT and ARHGAP42-ΔBAR, but not ARHGAP42-Y376F, stimulated the velocity of lamellipodial protrusions (Fig. 8C; Fig. S4B). Taken together, these results indicate that phosphorylation of ARHGAP42 Tyr-376 by Src can play an important role in stimulation of focal adhesion dynamics, lamellipodial velocity and cell migration.

DISCUSSION

ARHGAP42 (also known as GRAF3) was first revealed to be a target of tyrosine phosphorylation by phosphoproteomics studies. In addition to our previous study that identified ARHGAP42 as one of 32 known or putative Src substrates of known or likely biological relevance (Luo et al., 2008), ARHGAP42 was also recognized as one of 13 hyperphosphorylated proteins in fibroblasts deficient in the protein tyrosine phosphatase PTP1B (also known as PTPN1) (Mertins et al., 2008). At the time of these studies, ARHGAP42 was called 'similar to oligophrenin-1'. In both studies, the site of ARHGAP42 phosphorylation was identified as Tyr-376. Now, according to the PhosphoSitePlus database (http://www.phosphosite.org), ARHGAP42 Tyr-376 has been detected in >200 independent mass spectrometry studies that analyzed various cancer cell lines and disease tissues. The PhosphoSitePlus database also documents the frequent identification of corresponding residues on GRAF (Tyr-371) and oligophrenin-1 (Tyr-370) as sites of phosphorylation. Despite this abundance of data, there have been no published studies addressing how these tyrosine phosphorylation events might impact signaling functions. The primary objective of the present study was to evaluate ARHGAP42 Tyr-376 as a site of phosphorylation by Src and to investigate its possible regulatory role. By expressing WT mouse ARHGAP42 versus mutational variants, we have characterized ARHGAP42 as a regulator of cell motility that can be activated by Src-mediated phosphorylation of Tyr-376.

Journal of Cell Science (2017) 130, 2382-2393 doi:10.1242/jcs.197434

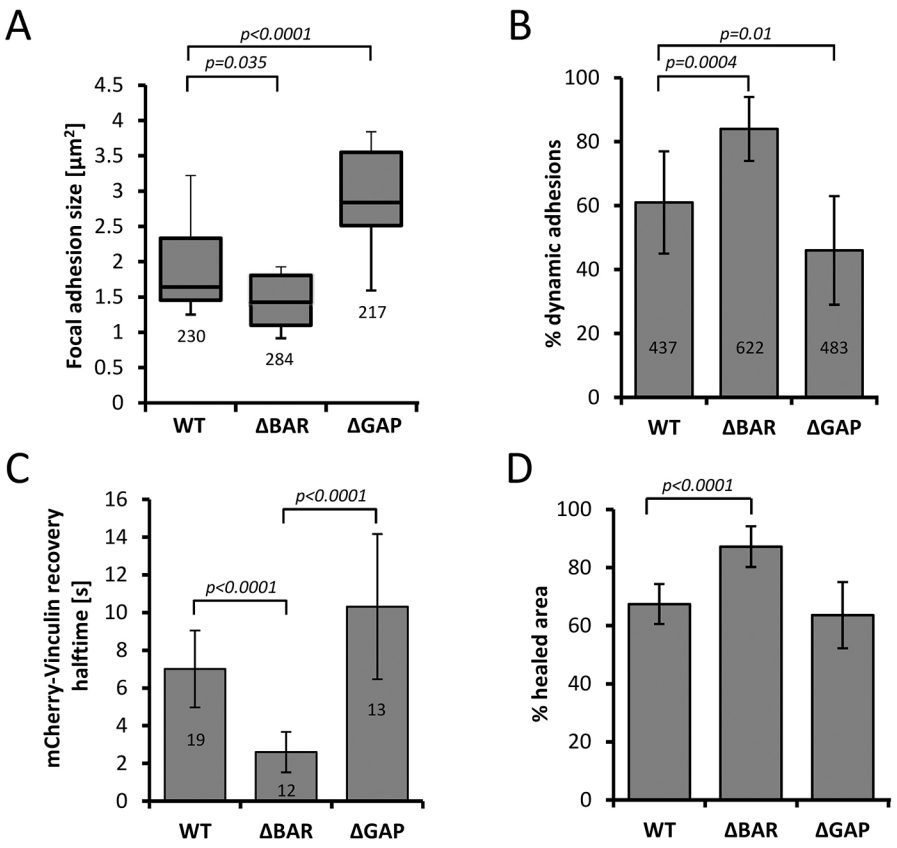

Fig. 5. Expression of ARHGAP42-ΔGAP increases focal adhesion size; expression of ARHGAP42-ΔBAR promotes focal adhesion turnover and cellular motility. (A) Quantification of focal adhesion size. MEFs expressing ARHGAP42 variants (WT, ΔBAR and ΔGAP) were grown on fibronectin-coated cover slips, fixed, immunostained with an antibody against paxillin, and focal adhesion size was analyzed by fluorescence microscopy. The box-and-whisker plot shows the range of size of focal adhesions. Center line shows the median, box limits indicate the first and third quartiles, whiskers extend to the minimum and maximum values. (B,C) MEFs were cotransfected with GFP-ARHGAP42 expression plasmids (WT, ΔBAR, ΔGAP) and (B) mCherry-zyxin or (C) mCherry-vinculin to mark focal adhesions. After transfection, cells were plated on fibronectin-coated glass bottom dishes and analyzed 48 h later by confocal live-cell microscopy. (B) The percentage of focal adhesions that either assembled or disassembled during a 20 min time interval. (C) FRAP analysis of mCherry-vinculin dynamics in focal adhesions, showing mean recovery halftimes. (A-C) The numbers in the histogram bars indicate the number of focal adhesions analyzed. (D) MEFs stably expressing GFP-ARHGAP42 variants (WT, ΔBAR, ΔGAP) were allowed to migrate for 24 h on a Petri dish and the healed area was subsequently determined by light microscopy followed by analysis using ImageJ software. Values are mean±s.d. Statistical significance was determined by one-way ANOVA followed by Tukey's post-hoc test.

ARHGAP42 is a member of a RhoGAP family characterized by N-terminal tandem BAR-PH domains followed by a central GAP domain with some specificity towards RhoA. In addition to BAR-PH and GAP domains, ARHGAP42 has an SH3 domain near the C-terminus. Of the three other mammalian members of this BAR-PH RhoGAP family, GRAF and PSGAP also have a C-terminal SH3 domain, but oligophrenin-1 does not. Nevertheless, phylogenetic analysis indicates that ARHGAP42 is more closely related to oligophrenin-1 than it is to GRAF and PSGAP, indicating that the loss of the oligophrenin-1 SH3 domain was a relatively recent evolutionary event.

By expressing GFP-tagged ARHGAP42 variants and detecting endogenous ARHGAP42 (Fig. S4C), we observed that ARHGAP42 localizes prominently in cells to actin stress fibers, which is consistent with a role for ARHGAP42 as an important regulator of actin cytoskeletal dynamics. The stress fiber localization requires the ARHGAP42 SH3 domain. Most likely the SH3 domain binds actin fibers indirectly through bridging proteins, such as is the case for the targeting of another BAR-GAP-SH3 protein, srGAP2, which binds via formin-like protein 1 (FMNL1) (Mason et al., 2011). In addition to stress fibers, ARHGAP42 was observed to variably localize to focal adhesions.

Previous *in vitro* studies demonstrated that the BAR domains of oligophrenin-1 and GRAF can interact directly, in *cis*, with their respective GAP domains to maintain the GAP domain in an autoinhibited state (Eberth et al., 2009). Our finding that expression of an ARHGAP42 variant with the BAR domain deleted gives rise to the arborized cell phenotype characteristic of RhoA/ROCK pathway inhibition indicates that the same autoinhibitory mechanism exists for ARHGAP42. With regard to this autoinhibitory function of the ARHGAP42 BAR domain, it is of interest that we obtained cDNAs encoding an alternate form of ARHGAP42 lacking 34 BAR domain residues (amino acids 129–162), but including much of the central BAR domain helix. It will be of interest for future studies to investigate the possibility that this alternative short form of ARHGAP42 has a constitutively active GAP domain.

We also presented evidence that the ability of the ARHGAP42 BAR-PH module to promote membrane tubulation in cells is enhanced when the GAP domain is deleted, suggesting that the GAP domain is also inhibitory to BAR-PH function. The apparent mutual inhibition of the BAR and GAP domains, however, stands in contrast to the findings of Eberth et al. (2009), showing that the BAR-PH domains of oligophrenin-1 and GRAF are not negatively impacted by the presence of the GAP domain. ARHGAP42 may have unique properties in this regard.

A role for the GAP activity of ARHGAP42 as a regulator of Rho-GTP levels and cytoskeletal or adhesion dynamics is evidenced by our findings that expression of the ARHGAP42 variant with the BAR domain deleted (and thus having elevated GAP activity) gives rise to increased focal adhesion dynamics, lamellipodial velocity and cell migration. These findings are in line with those of a recent study by Bai et al. (2013), which characterized ARHGAP42 as a RhoGAP expressed strongly in smooth muscle cells, and showed that depletion of the mouse *Arhgap42* gene resulted in a hypertensive phenotype with increased ROCK-dependent agonist-induced pressor responses.

To monitor the GAP activity of ARHGAP42, we employed two assays: a cell based assay analyzing arborized morphology induced by lowered RhoGTP levels, and a direct quantification of RhoGTP levels using a RhoGTP-pull-down approach. The effects of ARHGAP42 mutational variants were similar for both assays used, although their effects on arborized morphology were more prominent. However, similar results showing a mild decrease in

Journal of Cell Science (2017) 130, 2382-2393 doi:10.1242/jcs.197434

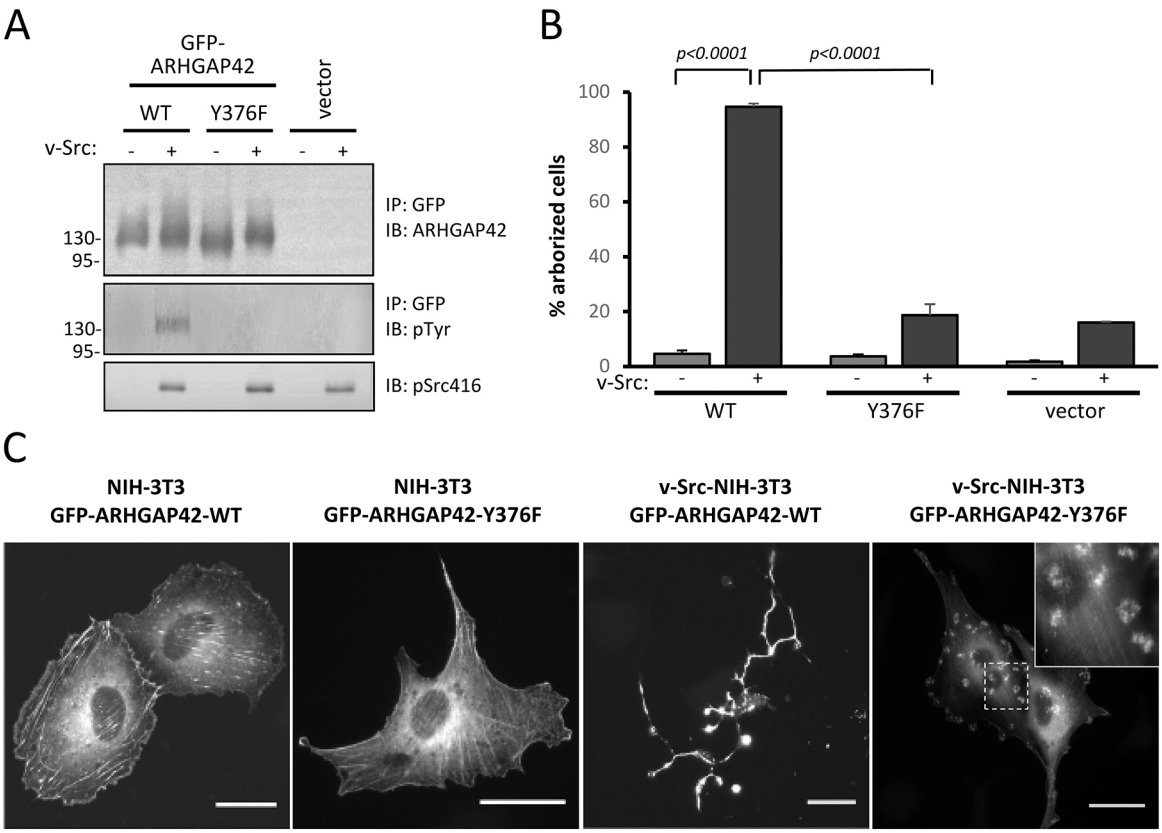

Fig. 6. Src activates the GAP activity of ARHGAP42, requiring the Tyr-376 phosphorylation site. GFP-ARHGAP42 variants, -WT versus -Y376F, were expressed in either nontransformed or v-Src-transformed NIH-3T3 fibroblasts and analyzed 24 h after transfection. (A) Expression and tyrosine phosphorylation of GFP-ARHGAP42 variants was assessed by IP using anti-GFP antibody, and IB with ARHGAP42 antibody (top panel) or anti-pTyr antibody (middle panel). Src activity is indicated by IB of whole cell lysates with antibody against the Src autophosphorylation site (bottom panel). (B) Quantitative analysis of the arborized morphology characteristic of RhoA inhibition in NIH-3T3 cells. Values are mean±s.d. from five independent transfection experiments, with 500 cells scored per experiment. Statistical significance was determined by one-way ANOVA followed by Tukey's post hoc test. (C) Subcellular localization of GFP-ARHGAP42 variants and cellular morphology were assessed by fluorescence microscopy of fixed cells. Representative nontransformed cells (left two panels) and v-Src-transformed cells (right two panels) are shown. The podosomal-like structures in the central region of a GFP-ARHGAP42-Y376F-expressing cell are shown in the inset. Scale bars: 30 µm.

RhoGTP levels leading to dramatic increase of the arborized phenotype have been observed (Noren et al., 2000). These could indicate that arborized morphology is induced only after some threshold level of RhoGTP is achieved.

We addressed the role of ARHGAP42 Tyr-376 phosphorylation as a critical regulator of ARHGAP42 activity by expressing WT versus Y376F variants of ARHGAP42 in cells with elevated Src activity, and monitoring the effects on cell shape and motility. In v-Src-transformed NIH-3T3 cells, expression of WT-ARHGAP42, but not Y376F-ARHGAP42, caused the cells to take on the highly arborized morphology indicative of elevated RhoGAP activity. In SYF cells that express Src-F529, the expression of WT-ARHGAP42, but not Y376F-ARHGAP42, resulted in decreased RhoA-GTP levels, while increasing focal adhesion dynamics, lamellipodial protrusion velocity, and cell migration. Notably, the effect of Tyr-376 phosphorylation mirrored the effect of the BAR domain deletion in promoting the GAP activity of ARHGAP42. Our findings add to a growing body of work documenting the role of protein phosphorylation in the regulation of BAR and F-BAR proteins (Ambroso et al., 2014; Quan et al., 2012; Roberts-Galbraith and Gould, 2010).

Our results suggest a phosphorylation model for the regulation of ARHGAP42 activity, whereby Src-mediated phosphorylation of ARHGAP42 Tyr-376 acts to disrupt the inhibitory effect of the BAR domain with the GAP domain, resulting in GAP domain activation, which reduces the levels of active GTP-bound RhoA and subsequently increases cell motility (Fig. S4D). In releasing the mutual inhibition of the BAR and GAP domains, Tyr-376 phosphorylation could also activate the membrane remodeling function for the ARHGAP42 BAR-PH domain.

MATERIALS AND METHODS

Mouse ARHGAP42 cDNA cloning and plasmids

A cDNA encoding full-length mouse ARHGAP42 was prepared from cultured MEFs using RT-PCR, with primers based on predicted N- and C-terminal coding regions. The forward primer (5′-AAGGTACC ATGGGGCTGCCCACTCTG-3′) incorporated a *KpnI* site prior to the start codon and the reverse primer (5′-GCGTCTAGATTAGAGGAAGAC AACGTAGTTTTCAGG-3′) incorporated an *XbaI* site following the stop codon. The amplified cDNA was then inserted into the *KpnI* and *XbaI* sites of cloning vector pBlueScript-SK+ for initial sequencing. For expression of mouse ARHGAP42 variants carrying an N-terminal GFP tag, vector pEGFP-C1 (Clontech) was used in the construction of plasmids pEGFP-C 1-mARHGAP42-WT, -ΔBAR, -ΔGAP, -ΔSH3, and -Y376F. Standard molecular methods were employed to introduce the individual deletions or point mutation. The three deletion variants lack amino acid residues 1–249 (ΔBAR), 388–576 (ΔGAP), or 819–875 (ΔSH3). For retroviral infection, the

Journal of Cell Science (2017) 130, 2382-2393 doi:10.1242/jcs.197434

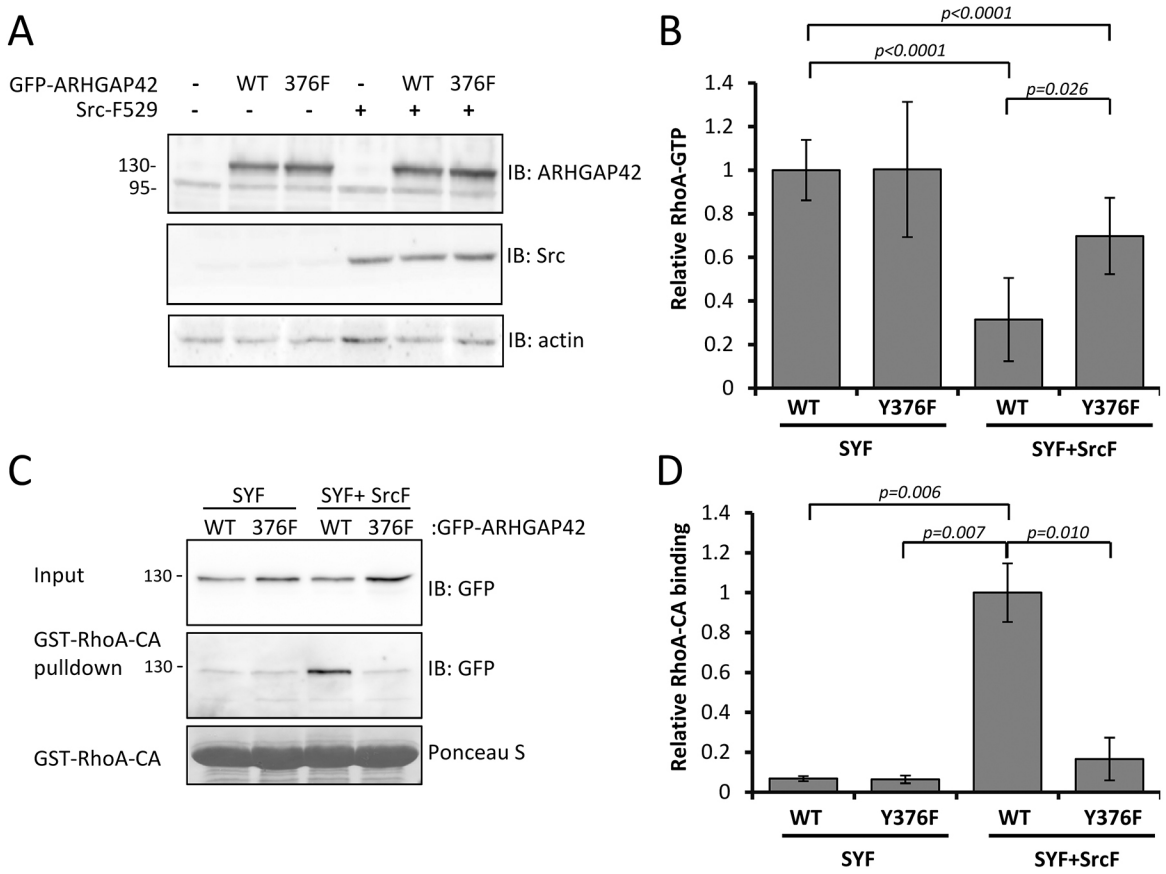

Fig. 7. Src phosphorylation on Tyr376 regulates ARHGAP42 activity. SYF cells or SYF cells expressing constitutively active Src-F529 (SrcF) were transfected to stably express GFP-ARHGAP42-WT versus -Y376F. (A) Expression of ARHGAP42 and Src was confirmed by IB, with actin (bottom) as a control for equal loading. The ARHGAP42 antibody detects the GFP-tagged variants as well as an additional band of expected size for the endogenous protein. (B) Relative RhoA-GTP levels were determined in cell lysates using the G-LISA assay. Values are mean±s.d. RhoA-GTP signal compared to the signal from ARHGAP42-WT-expressing cells, from three independent experiments performed in triplicate. (C) The ability of ARHGAP42 to bind RhoA-CA was analyzed using a GST-RhoA-CA pull-down assay and (D) quantified as a ratio of the amount of indicated GFP-ARHGAP42 variant pulled down with GST-RhoA-CA and the corresponding amount of GFP-ARHGAP42 in the input cell lysate. Statistical significance was determined by one-way ANOVA followed by Tukey's post-hoc test.

individual ARHGAP42 variants including the EGFP were PCR amplified from the corresponding pEGFP-C1 plasmids using a forward primer (5′-C TGCATGATCAGCCACCATGGTGAGCAAGGGC-3′) and a reverse primer (5′- CAGGTCAATTGTTAGAGGAAGACAACGTAGTT-3′). The amplified cDNAs were then cleaved with *BclI* and *MunI* and inserted into the *BglII* and *EcoRI* sites of pMSCV-puro vector. The resulting constructs were verified by sequencing. Plasmids pCMV-N2-mARHGAP42-HA-WT, -ΔBAR, -ΔSH3, and -Y376F were constructed for expression of mouse ARHGAP42 variants carrying a triple-HA epitope tag at their C-terminal ends; these plasmids were derived from vector pEGFP-N2 (Clontech), with the EGFP coding segment replaced with the sequence for the triple-HA tag. Plasmid pGEX-KG-mARHGAP42GAP was constructed for bacterial expression of the mouse ARHGAP42 GAP domain (amino acid residues 384–583). For construction of pMSCV-puro-Src-529F, Src-529F was recloned from source vector pBluescriptII-Src-529F (Brábek et al., 2002) using *NotI* (blunt ended) and *BamHI* restriction endonucleases, and the generated fragment was inserted to *HpaI* and *BglII* sites of pMSCV-puro vector. Plasmid mCherry-C1-zyxin was a gift from Irina Kaverina (Vanderbilt University, Nashville, TN).

Antibodies

A rabbit polyclonal antibody against mouse ARHGAP42 was custom made by Pacific Immunology (Ramona, CA) using a bacterially expressed immunogen-encompassing mouse ARHGAP42 (amino acid residues 580–820, a poorly conserved region between the GAP and SH3 domains) (at dilution 1:500). The monoclonal antibody against paxillin was from BD Transduction Laboratories (cat. no. 610051, 1:1,000) monoclonal antibodies against phospho-paxillin (cat. no. 07-1440, 1:1,000) and β actin (cat. no. A5316, 1:5,000) were from Sigma-Aldrich. The polyclonal anti-GFP antibody used for immunoblotting was from Thermo Fisher Scientific (cat. no. A-6455, 1:1,000), and the monoclonal anti-GFP 3E6 used for immunoprecipitation was from Invitrogen (cat. no. A-11120, 1:1,000). Anti-pTyr antibody 4G10 (cat. no. 05-321, 1:1,000) and v-Src antibody 327 (cat. no. OP07, 1:1,000) were from EMD Millipore. Rabbit monoclonal antibody against RhoA (cat. no. 2117, 1:1,000), and phosphospecific antibodies against Src-pTyr416 (cat. no. 6943, 1:1,000) and ARHGAP42-pTyr376 (cat. no. 5617, 1:1,000) were all obtained from Cell Signaling Technology.

Rho GTPase assay

The GAP domain of mouse ARHGAP42 was expressed from plasmid pGEX-KG-mARHGAP42GAP in bacterial strain BL21(DE3) as a GST-fusion protein and purified using glutathione agarose beads (Sigma-Aldrich). Protein was eluted from the beads using 0.25% glutathione and concentrated in 50 mM Tris-HCl, 50 mM NaCl and 5 mM EDTA (pH 7.5) to a final volume of 200 µl. Activity was assayed with a RhoGAP ASSAY, Biochem Kit (Cytoskeleton) according to the manufacturer's protocol. Briefly, 8 µg of protein was incubated in the presence of different recombinant GTPases, GTP and optimized buffer. The amount of released inorganic phosphate, the product of GTP hydrolysis, was measured by absorbance at 650 nm.

Cell culture and transfection

All cell lines were cultured in full DMEM (Life Technologies) with 4.5 g/l L-glucose, L-glutamine and pyruvate, supplemented with 10% fetal bovine serum (Sigma-Aldrich), 2% antibiotic–antimycotic (Life Technologies),

Journal of Cell Science (2017) 130, 2382-2393 doi:10.1242/jcs.197434

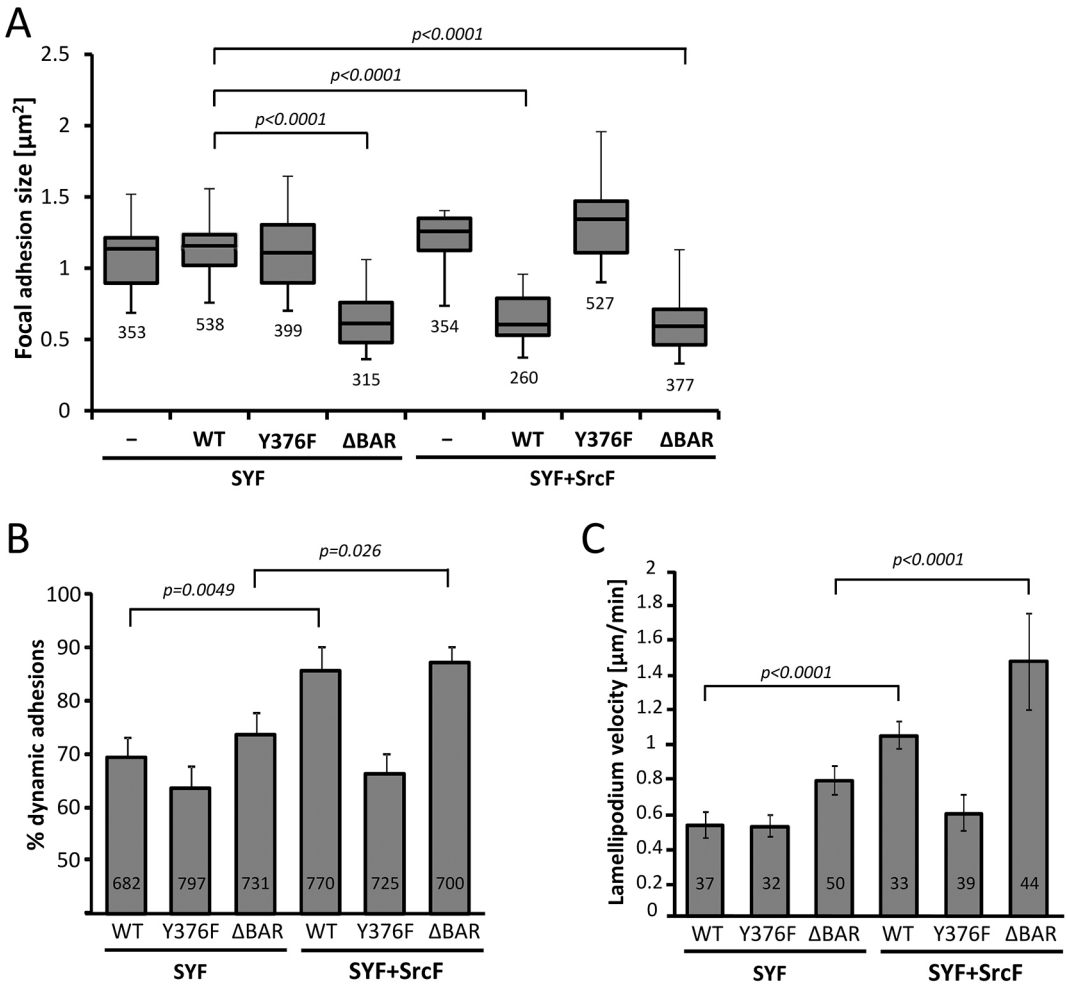

Fig. 8. Src phosphorylation of ARHGAP42 on Tyr376 regulates focal adhesion size and dynamics of lamellipodia and focal adhesions. SYF cells or SYF cells expressing constitutively active Src-F529 (SrcF) were cotransfected with GFP-ARHGAP42 expression plasmids (WT, Y376F and ΔBAR), and plated on fibronectin-covered glass bottom dishes. At 24 h, cells showing similar levels of GFP-ARHGAP42 fluorescence, judged using an integrated intensity value of the GFP signal per cell and acquired with same settings (exposure, laser power, detector gain, etc.) of the microscope, were analyzed by confocal cell microscopy. (A) Quantitative analysis of focal adhesion size. The box-and-whisker plot shows the range in size of focal adhesions marked by paxillin staining in fixed cells. (B) Quantitative analysis of focal adhesion dynamics in live cells. Values are mean±s.e.m. percentage of dynamic focal adhesions during a 10 min time interval. (A,B) The numbers in the indicate the number of focal adhesions analyzed. (C) Quantitative analysis of lamellipodia velocities. Values are mean±s.e.m. velocities of protruding lamellipodia. The numbers in the histogram bars indicate the number of cells analyzed. Statistical significance was determined by one-way ANOVA followed by Tukey's post-hoc test.

and 1% MEM nonessential amino acids (Life Technologies). Cell transfections were carried out using either Lipofectamine-2000 (Thermo Fisher Scientific) or Polyethylenimine-PEI (Sigma-Aldrich) according to the manufacturers' protocols. For some experiments, stable cell lines were prepared using plasmids pMSCV-puro-GFP-ARHGAP42-WT; -ΔBAR; -ΔGAP; -Y376F and the Phoenix retroviral packaging lineage, followed by fluorescence-activated cell sorting (FACS) for GFP. SYF fibroblasts stably expressing Src-529F were prepared via retrovirus infection using pMSCV-puro-Src-529F vector and Phoenix packaging lineage with subsequent puromycin selection.

Cell immunostaining and fluorescence microscopy

Transfected cells were seeded on coverslips coated with human fibronectin 10 µg/ml (Invitrogen), grown for 24–48 h, and subsequently fixed in 4% paraformaldehyde in 127 mM NaCl, 5 mM KCl, 1.1 mM NaH_2PO_4, 0.4 mM KH_2PO_4 and 20 mM HEPES (pH 7.1), permeabilized in 0.5% Triton X-100 in PBS, washed extensively with PBS, and blocked in 3% BSA in PBS. The cells were then sequentially incubated with the primary antibody against paxillin for 2 h, secondary antibody for 60 min and phalloidin Dy-405 (Dyomics) for 15 min, with extensive washing between each step. The secondary antibodies were anti-rabbit-IgG Alexa Fluor 546-conjugated antibody and anti-mouse-IgG Alexa Fluor 594- and Alexa Fluor 633-conjugated antibodies (Molecular Probes). Images were acquired by Leica TCS SP2 or TCS SP8 microscope systems equipped with a Leica 63×/1.45 NA oil objective.

Quantification of GFP-ARHGAP42 localization to focal adhesions

Focal adhesions indicated by paxillin staining were detected automatically using ImageJ according to Horzum et al., (2014). Focal adhesions were considered positive for GFP-ARHGAP42 if the GFP signal in focal adhesion was ≥20% higher than the average GFP signal in cytoplasm.

Immunoprecipitation and immunoblotting

Subconfluent cell cultures were washed with PBS and lysed in modified RIPA buffer [0.15 M NaCl, 50 mM Tris-HCl (pH 7.4), 1% Nonidet P-40, 0.1% SDS, 1% sodium deoxycholate, 5 mM EDTA and 50 mM NaF]. Protein concentrations in lysates were determined using the DC Protein Assay (Bio-Rad). Lysates equivalent to 20 µg protein were diluted in 2× Laemmli sample buffer [0.35 M Tris-HCl (pH 6.8), 10% SDS, 40% glycerol and 0.012% Bromophenol Blue] for immunoblot analysis of whole

cell extracts. Immunoprecipitations were carried out from 1 ml RIPA lysates containing equal amounts of total protein (200–500 µg). Lysates were incubated 4 h on ice with 1 µg primary antibody and immune complexes were collected by an additional 1 h incubation with protein G-Sepharose (20 µl 50% slurry). The immunoprecipitates were washed five times with 1 ml ice-cold RIPA buffer, resuspended in 2× SDS-PAGE sample buffer and processed for immunoblotting. For immunoblotting, samples were separated on SDS polyacrylamide gels (ranging from 7.5% to 15%), transferred to nitrocellulose membranes, and nonspecific activity was blocked by incubating the membranes for 90 min at room temperature in Tris-buffered saline containing 4% BSA. Membranes were then incubated overnight at 4°C with a primary antibody, washed extensively with Tris-buffered saline with Tween-20 (TTBS), incubated for 1 h at room temperature with HRP-conjugated secondary antibodies (Sigma-Aldrich) at 1:10,000 washed extensively in TTBS, and developed using either an Odyssey or Fuji LAS chemiluminescence imaging system. Western blot quantification was performed using ImageJ software (http://rsbweb.nih.gov/ij/).

Kinase assay

GFP-ARHGAP42 variants were immunoprecipitated from MEFs using anti-GFP antibody (Invitrogen), SrcF was immunoprecipitated from MEFs using v-Src antibody (EMD Millipore). The GFP-ARHGAP42 variants were eluted from the slurry using 0.1 M glycine pH 3.5 followed by neutralization with 1 M Tris-HCl pH 9.2 (1/20 of total volume). Precipitated GFP-ARHGAP42 variants were transferred to Src529F (bound on protein G-Sepharose) in kinase buffer (50 mM HEPES pH 7.4, 1% Triton X-100, 1 mM DTT, 6 mM $MgCl_2$, 6 mM $MnCl_2$, 100 µM ATP, 200 µM orthovanadate and protease inhibitors) and incubated on a rotator at 30°C for the indicated times (0.5, 1, 1.5 and 2 h). The reaction was stopped by adding 6× SDS-PAGE sample buffer and boiling for 5 min.

RhoA activation assay

Cells were grown to 70% confluency and then incubated overnight in serum-free medium. The cells were then serum stimulated by incubating for 3 min in DMEM containing 10% FBS, then washed in ice-cold PBS. Lysis buffer (G-LISA RhoA Activation Assay, Cytoskeleton) was added, and immediately the cells were scraped and lysates were centrifuged for 2 min at 9,300 ***g***. Aliquots for estimating protein concentration were collected, and the remaining lysates were snap-frozen in liquid nitrogen prior to being assessed for RhoA activity using the G-LISA assay according to the manufacturer's protocol.

RhoA pull-down assay

A constitutively active form of RhoA (RhoA-CA, G14V) was PCR amplified with a forward primer encoding *BamHI* (5′-ATTGGATCCCGG ATGGCTG-3′) and a reverse primer encoding *EcoRI* site (5′-GCAG AATTCCTCACAAGACCAG-3′) and subcloned into pGEX-2T bacterial expression vector via *BamHI* and *EcoRI* sites. GST-fused RhoA-CA was expressed in *E. coli* BL21(DE3) strain and affinity purified using Pierce Glutathione Agarose (Thermo Fisher Scientific). The RhoA pull-down assay was performed as described in García-Mata et al. (2006). Briefly, cells were washed twice with ice-cold HBS (20 mM HEPES pH 7.5, 150 mM NaCl) and lysed in HBS containing 1% Triton X-100, 5 mM $MgCl_2$ and 1 mM DTT supplied with inhibitors of proteases (Mix M, SERVA) and phosphatases (Mix-II, SERVA). The lysates were equalized for the total amount of GFP-ARHGAP42. Agarose-bound RhoA-CA (15 µg) was added to each lysate and rotated for 1 h at 4°C. The beads were then washed three times in lysis buffer and resuspended in SDS-PAGE sample buffer. The samples were resolved and analyzed by immunoblotting as described above.

Live-cell microscopy

MEFs were cotransfected with pEGFP-C1-mARHGAP42 variants and mCherry-C1-zyxin (focal adhesion marker), and 24 h later were transferred to glass bottom dishes (Ibidi). Cells were kept in Phenol Red-free DMEM supplemented with 10% FBS and 2% antibiotics-antimycotics mix. Motile cells were observed in red fluorescence channel for focal adhesion dynamics experiments, or using internal reflection microscopy mode for lamellipodial dynamics experiments at 37°C and 5% CO_2. Images were taken at 30 s intervals for a total of 20 min using a Leica TCS SP2 microscope system equipped with a Leica 63×/1.45 NA oil objective and a Zeiss LSM 880 confocal microscope, equipped with a Zeiss 63×/1.45 NA oil objective. Focal adhesion dynamics analysis was performed according to Webb et al. (2004). For kymograph analysis, ImageJ software was used to draw three lines (1 pixel wide, 0.22 mm) per lamellipodium in the direction of the protrusion. The lamellipodium velocities were calculated from kymographs using the kymograph plugin for ImageJ (J. Rietdorf, FMI Basel, and A. Seitz, EMBL Heidelberg; https://www.embl.de/eamnet/html/body_kymograph.html).

FRAP

FRAP experiments were performed on a Leica SP8 confocal microscope with a 63×/1.2 NA water immersion objective. Cells were cotransfected with mCherry-vinculin and GFP-ARHGAP42 variants. After 2 days, cells were transferred to 35 mm dishes (MatTek) and cultured overnight, and then used for FRAP analysis. A 584 nm white light laser was used for mCherry excitation and bleaching was performed with simultaneous excitation using 576 nm and 584 set on 100% of the fluorescence intensity for 5 s. The image acquisition started 3 s before bleaching and continued for approximately 60 s (one frame every 1.048 s). The recovery curves of the bleached regions were calculated from extracted image series, and the recovery halftime values were calculated from the FRAP curves as described in Tolde et al. (2012).

Wound healing assay

Cells were grown to full confluency and a wound was made in the confluent monolayer using a plastic 1 ml pipette tip. Immediately after the wounding, and again after 24 h in culture, ≥15 images of different areas were acquired using a Nikon Eclipse TE2000-S (10×/0.25 NA Plan Fluor objective). Cell-free areas were measured using ImageJ software and quantified.

Acknowledgements

We thank Professor Jan Černý for valuable discussions and comments.

Competing interests

The authors declare no competing or financial interests.

Author contributions

Conceptualization: R.J., J.B., S.K.H., D.R.; Formal analysis: W.L., R.J., O.T., L.M.R., L.K., M.D., S.K.H., D.R.; Investigation: W.L., R.J., O.T., L.M.R., L.K., M.D.; Resources: J.B., S.K.H., D.R.; Writing - original draft: W.L., R.J., O.T., L.M.R., J.B., S.K.H., D.R.; Writing - review & editing: W.L., R.J., O.T., J.B., S.K.H., D.R.; Visualization: W.L., R.J., O.T., S.K.H., D.R.; Supervision: J.B., S.K.H., D.R.; Project administration: J.B., S.K.H., D.R.; Funding acquisition: J.B., S.K.H., D.R.

Funding

This work was funded by the National Institutes of Health (R01-GM049882), Vanderbilt-Ingram Cancer Center (5P30-CA068485), Grantová Agentura České Republiky (Czech Science Foundation) (15-07321S), and Ministerstvo Školství, Mládeže a Tělovýchovy (Ministry of Education, Youth and Sports of the Czech Republic), within the LQ1604 National Sustainability Program II (Project BIOCEV-FAR) and the project BIOCEV (CZ.1.05/1.1.00/02.0109 and LM2015062, Czech-BioImaging). Deposited in PMC for release after 12 months.

Supplementary information

Supplementary information available online at
http://jcs.biologists.org/lookup/doi/10.1242/jcs.197434.supplemental

References

Ambroso, M. R., Hegde, B. G. and Langen, R. (2014). Endophilin A1 induces different membrane shapes using a conformational switch that is regulated by phosphorylation. *Proc. Natl. Acad. Sci. USA* **111**, 6982-6987.

Arthur, W. T., Petch, L. A. and Burridge, K. (2000). Integrin engagement suppresses RhoA activity via a c-Src-dependent mechanism. *Curr. Biol.* **10**, 719-722.

Bai, X., Lenhart, K. C., Bird, K. E., Suen, A. A., Rojas, M., Kakoki, M., Li, F., Smithies, O., Mack, C. P. and Taylor, J. M. (2013). The smooth muscle-selective RhoGAP GRAF3 is a critical regulator of vascular tone and hypertension. *Nat. Commun.* **4**, 2910.

Bass, M. D., Morgan, M. R., Roach, K. A., Settleman, J., Goryachev, A. B. and Humphries, M. J. (2008). p190RhoGAP is the convergence point of adhesion signals from alpha 5 beta 1 integrin and syndecan-4. *J. Cell Biol.* **181**, 1013-1026.
Billuart, P., Bienvenu, T., Ronce, N., des, P. V., Vinet, M. C., Zemni, R., Carrie, A., Beldjord, C., Kahn, A., Moraine, C. et al. (1998). Oligophrenin 1 encodes a rho-GAP protein involved in X-linked mental retardation. *Pathol. Biol. (Paris)* **46**, 678.
Brábek, J., Mojžita, D., Novotný, M., Půta, F. and Folk, P. (2002). The SH3 domain of Src can downregulate its kinase activity in the absence of the SH2 domain-pY527 interaction. *Biochem. Biophys. Res. Commun.* **296**, 664-670.
Cheresh, D. A., Leng, J. and Klemke, R. L. (1999). Regulation of cell contraction and membrane ruffling by distinct signals in migratory cells. *J. Cell Biol.* **146**, 1107-1116.
Corpet, F. (1988). Multiple sequence alignment with hierarchical clustering. *Nucleic Acids Res.* **16**, 10881-10890.
Eberth, A., Lundmark, R., Gremer, L., Dvorsky, R., Koessmeier, K. T., McMahon, H. T. and Ahmadian, M. R. (2009). A BAR domain-mediated autoinhibitory mechanism for RhoGAPs of the GRAF family. *Biochem. J.* **417**, 371-379.
Eden, S., Rohatgi, R., Podtelejnikov, A. V., Mann, M. and Kirschner, M. W. (2002). Mechanism of regulation of WAVE1-induced actin nucleation by Rac1 and Nck. *Nature* **418**, 790-793.
Fincham, V. J. and Frame, M. C. (1998). The catalytic activity of Src is dispensable for translocation to focal adhesions but controls the turnover of these structures during cell motility. *EMBO J.* **17**, 81-92.
Fincham, V. J., Chudleigh, A. and Frame, M. C. (1999). Regulation of p190 Rho-GAP by v-Src is linked to cytoskeletal disruption during transformation. *J. Cell Sci.* **112**, 947-956.
Frame, M. C. (2004). Newest findings on the oldest oncogene; how activated src does it. *J. Cell Sci.* **117**, 989-998.
Frame, M. C., Fincham, V. J., Carragher, N. O. and Wyke, J. A. (2002). v-Src's hold over actin and cell adhesions. *Nat. Rev. Mol. Cell Biol.* **3**, 233-245.
García-Mata, R., Wennerberg, K., Arthur, W. T., Noren, N. K., Ellerbroek, S. M. and Burridge, K. (2006). Analysis of activated GAPs and GEFs in cell lysates. *Methods Enzymol.* **406**, 425-437.
Hanks, S. K., Ryzhova, L., Shin, N. Y. and Brabek, J. (2003). Focal adhesion kinase signaling activities and their implications in the control of cell survival and motility. *Front. Biosci.* **8**, d982-d996.
Hildebrand, J. D., Taylor, J. M. and Parsons, J. T. (1996). An SH3 domain-containing GTPase-activating protein for Rho and Cdc42 associates with focal adhesion kinase. *Mol. Cell Biol.* **16**, 3169-3178.
Horzum, U., Ozdil, B. and Pesen-Okvur, D. (2014). Step-by-step quantitative analysis of focal adhesions. *MethodsX.* **1**, 56-59.
Huveneers, S. and Danen, E. H. J. (2009). Adhesion signaling-crosstalk between integrins, Src and Rho. *J. Cell Sci.* **122**, 1059-1069.
Jiang, W., Betson, M., Mulloy, R., Foster, R., Levay, M., Ligeti, E. and Settleman, J. (2008). p190A RhoGAP is a glycogen synthase kinase-3-beta substrate required for polarized cell migration. *J. Biol. Chem.* **283**, 20978-20988.
Kim, D.-H. and Wirtz, D. (2013). Focal adhesion size uniquely predicts cell migration. *FASEB J.* **27**, 1351-1361.
Kiyokawa, E., Hashimoto, Y., Kobayashi, S., Sugimura, H., Kurata, T. and Matsuda, M. (1998). Activation of Rac1 by a Crk SH3-binding protein, DOCK180. *Genes Dev.* **12**, 3331-3336.
Klemke, R. L., Leng, J., Molander, R., Brooks, P. C., Vuori, K. and Cheresh, D. A. (1998). CAS/Crk coupling serves as a "molecular switch" for induction of cell migration. *J. Cell Biol.* **140**, 961-972.
Klinghoffer, R. A., Sachsenmaier, C., Cooper, J. A. and Soriano, P. (1999). Src family kinases are required for integrin but not PDGFR signal transduction. *EMBO J.* **18**, 2459-2471.
Lessey, E. C., Guilluy, C. and Burridge, K. (2012). From mechanical force to RhoA activation. *Biochemistry* **51**, 7420-7432.
Li, J., Mao, X., Dong, L. Q., Liu, F. and Tong, L. (2007). Crystal structures of the BAR-PH and PTB domains of human APPL1. *Structure* **15**, 525-533.
Lundmark, R., Doherty, G. J., Howes, M. T., Cortese, K., Vallis, Y., Parton, R. G. and McMahon, H. T. (2008). The GTPase-activating protein GRAF1 regulates the CLIC/GEEC endocytic pathway. *Curr. Biol.* **18**, 1802-1808.
Luo, W., Slebos, R. J., Hill, S., Li, M., Brábek, J., Amanchy, R., Chaerkady, R., Pandey, A., Ham, A.-J. L. and Hanks, S. K. (2008). Global impact of oncogenic Src on a phosphotyrosine proteome. *J. Proteome. Res.* **7**, 3447-3460.
Mason, F. M., Heimsath, E. G., Higgs, H. N. and Soderling, S. H. (2011). Bi-modal regulation of a formin by srGAP2. *J. Biol. Chem.* **286**, 6577-6586.
Mertins, P., Eberl, H. C., Renkawitz, J., Olsen, J. V., Tremblay, M. L., Mann, M., Ullrich, A. and Daub, H. (2008). Investigation of protein-tyrosine phosphatase 1B function by quantitative proteomics. *Mol. Cell Proteomics.* **7**, 1763-1777.
Miki, H., Yamaguchi, H., Suetsugu, S. and Takenawa, T. (2000). IRSp53 is an essential intermediate between Rac and WAVE in the regulation of membrane ruffling. *Nature* **408**, 732-735.
Nojima, Y., Morino, N., Mimura, T., Hamasaki, K., Furuya, H., Sakai, R., Sato, T., Tachibana, K., Morimoto, C., Yazaki, Y. et al. (1995). Integrin-mediated cell adhesion promotes tyrosine phosphorylation of p130Cas, a Src homology 3-containing molecule having multiple Src homology 2-binding motifs. *J. Biol. Chem.* **270**, 15398-15402.
Noren, N. K., Liu, B. P., Burridge, K. and Kreft, B. (2000). p120 catenin regulates the actin cytoskeleton via Rho family GTPases. *J. Cell Biol.* **150**, 567-580.
Omelchenko, T., Vasiliev, J. M., Gelfand, I. M., Feder, H. H. and Bonder, E. M. (2002). Mechanisms of polarization of the shape of fibroblasts and epitheliocytes: separation of the roles of microtubules and Rho-dependent actin-myosin contractility. *Proc. Natl. Acad. Sci. USA* **99**, 10452-10457.
Peter, B. J., Kent, H. M., Mills, I. G., Vallis, Y., Butler, P. J., Evans, P. R. and McMahon, H. T. (2004). BAR domains as sensors of membrane curvature: the amphiphysin BAR structure. *Science* **303**, 495-499.
Prakash, S. K., Paylor, R., Jenna, S., Lamarche-Vane, N., Armstrong, D. L., Xu, B., Mancini, M. A. and Zoghbi, H. Y. (2000). Functional analysis of ARHGAP6, a novel GTPase-activating protein for RhoA. *Hum. Mol. Genet.* **9**, 477-488.
Quan, A., Xue, J., Wielens, J., Smillie, K. J., Anggono, V., Parker, M. W., Cousin, M. A., Graham, M. E. and Robinson, P. J. (2012). Phosphorylation of syndapin I F-BAR domain at two helix-capping motifs regulates membrane tubulation. *Proc. Natl. Acad. Sci. USA* **109**, 3760-3765.
Raftopoulou, M. and Hall, A. (2004). Cell migration: Rho GTPases lead the way. *Dev. Biol.* **265**, 23-32.
Ren, X. D., Kiosses, W. B., Sieg, D. J., Otey, C. A., Schlaepfer, D. D. and Schwartz, M. A. (2000). Focal adhesion kinase suppresses Rho activity to promote focal adhesion turnover. *J. Cell Sci.* **113**, 3673-3678.
Ren, X.-R., Du, Q.-S., Huang, Y.-Z., Ao, S.-Z., Mei, L. and Xiong, W.-C. (2001). Regulation of CDC42 GTPase by proline-rich tyrosine kinase 2 interacting with PSGAP, a novel pleckstrin homology and Src homology 3 domain containing rhoGAP protein. *J. Cell Biol.* **152**, 971-984.
Ridley, A. J., Paterson, H. F., Johnston, C. L., Diekmann, D. and Hall, A. (1992). The small GTP-binding protein rac regulates growth factor-induced membrane ruffling. *Cell* **70**, 401-410.
Roberts-Galbraith, R. H. and Gould, K. L. (2010). Setting the F-BAR: functions and regulation of the F-BAR protein family. *Cell Cycle* **9**, 4091-4097.
Rosel, D., Brabek, J., Vesely, P. and Fernandes, M. (2013). Drugs for solid cancer: the productivity crisis prompts a rethink. *Onco. Targets. Ther.* **6**, 767-777.
Rottner, K., Hall, A. and Small, J. V. (1999). Interplay between Rac and Rho in the control of substrate contact dynamics. *Curr. Biol.* **9**, 640-648.
Schlaepfer, D. D., Hanks, S. K., Hunter, T. and van der Geer, P. (1994). Integrin-mediated signal transduction linked to Ras pathway by GRB2 binding to focal adhesion kinase. *Nature* **372**, 786-791.
Sharma, A. and Mayer, B. J. (2008). Phosphorylation of p130Cas initiates Rac activation and membrane ruffling. *BMC. Cell Biol.* **9**, 50.
Shibata, H., Oishi, K., Yamagiwa, A., Matsumoto, M., Mukai, H. and Ono, Y. (2001). PKNbeta interacts with the SH3 domains of Graf and a novel Graf related protein, Graf2, which are GTPase activating proteins for Rho family. *J. Biochem.* **130**, 23-31.
Tatsis, N., Lannigan, D. A. and Macara, I. G. (1998). The function of the p190 Rho GTPase-activating protein is controlled by its N-terminal GTP binding domain. *J. Biol. Chem.* **273**, 34631-34638.
ten Klooster, J. P., Jaffer, Z. M., Chernoff, J. and Hordijk, P. L. (2006). Targeting and activation of Rac1 are mediated by the exchange factor beta-Pix. *J. Cell Biol.* **172**, 759-769.
Tolde, O., Rosel, D., Janostiak, R., Vesely, P. and Brabek, J. (2012). Dynamics and morphology of focal adhesions in complex 3D environment. *Folia Biol.* **58**, 177-184.
Webb, D. J., Donais, K., Whitmore, L. A., Thomas, S. M., Turner, C. E., Parsons, J. T. and Horwitz, A. F. (2004). FAK-Src signalling through paxillin, ERK and MLCK regulates adhesion disassembly. *Nat. Cell Biol.* **6**, 154-161.
Welch, M. D. and Mullins, R. D. (2002). Cellular control of actin nucleation. *Annu. Rev. Cell Dev. Biol.* **18**, 247-288.
Zhu, G., Chen, J., Liu, J., Brunzelle, J. S., Huang, B., Wakeham, N., Terzyan, S., Li, X., Rao, Z., Li, G. et al. (2007). Structure of the APPL1 BAR-PH domain and characterization of its interaction with Rab5. *EMBO J.* **26**, 3484-3493.

Supplemental Figure S1.

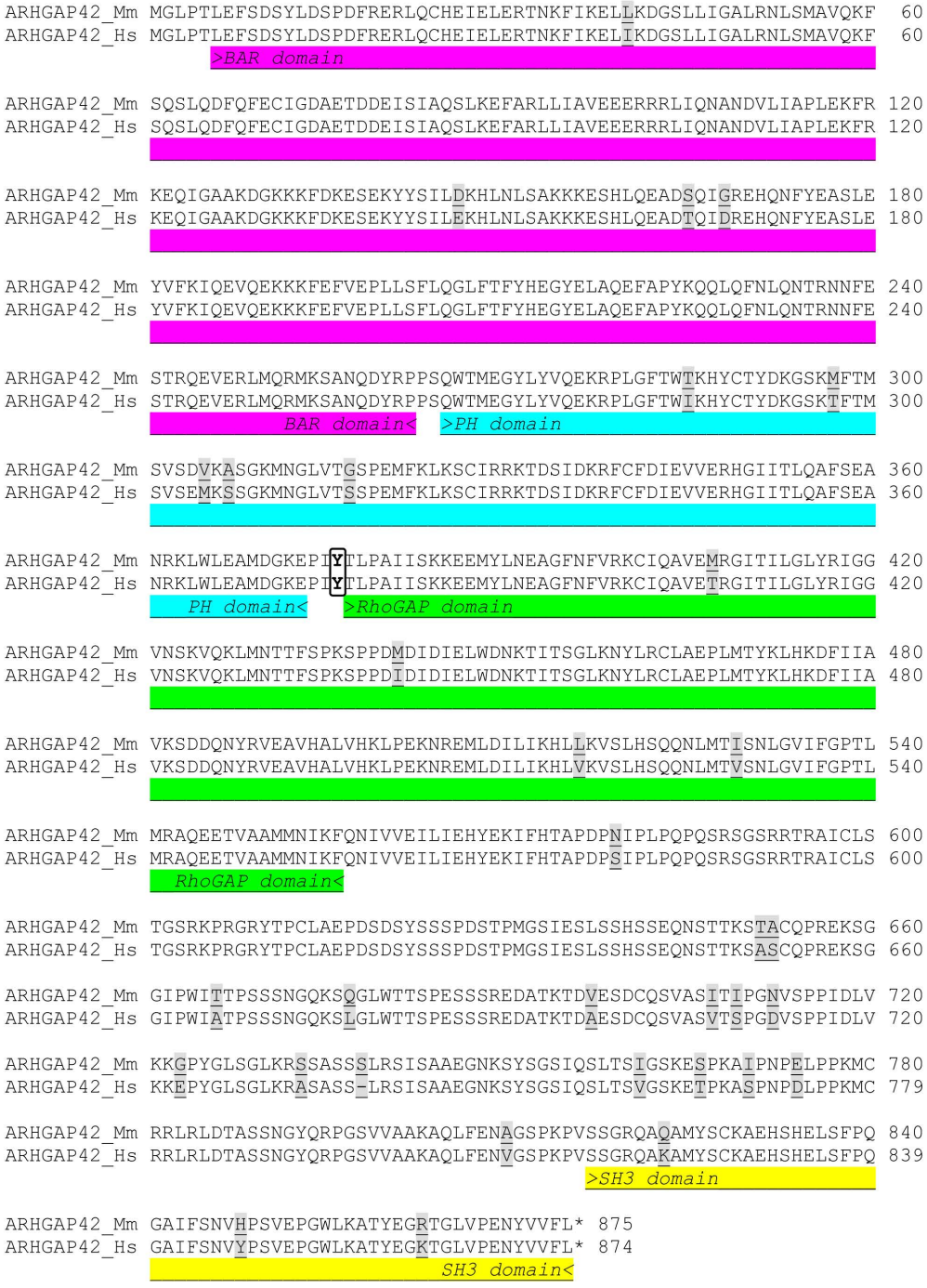

Supplemental Figure S1. Mouse *vs.* human ARHGAP42. Mouse ARHGAP42 (ARHGAP42_Mm) is shown aligned against the predicted human protein (ARHGAP42_Hs; UniProt accession number A6NI28). Non-identical residues are shaded. Asterisks indicate STOP codons. Numbers indicate amino acid position. Positions of BAR, PH, GAP, and SH3 domains are shown below the aligned sequences. The Tyr-376 phosphorylation site is in bold and indicated by a box. Note that the UniProt entry for mouse RhoGAP42 (accession number B2RQE8, not shown) is missing amino acid residues 129-162 within the BAR domain.

Supplemental Figure S2.

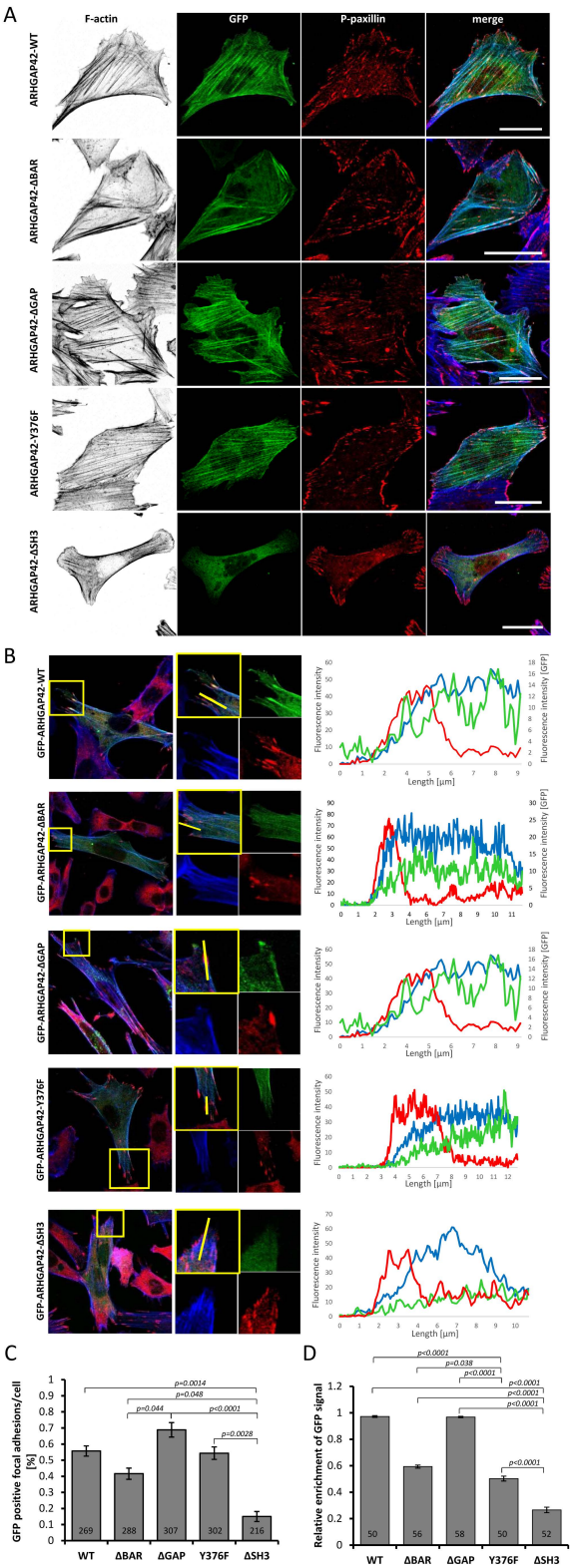

Supplemental Figure S2. Subcellular localization of ARHGAP42 mutational variants. (A) GFP-ARHGAP42 variants ΔBAR, ΔGAP, ΔSH3, and Y376F were expressed in MEFs and analyzed by fluorescence microscopy. The cells were immunostained with phalloidin to mark F-actin (in grey or blue), anti phospho-paxillin antibody to mark focal adhesions (in red) and GFP-ARHGAP42 variants were visualized by GFP fluorescence (in green). Scale bars are 30 µm. (B) Analysis of GFP-ARHGAP42 variants localization to focal adhesions. MEFs expressing indicated ARHGAP42 variants were prepared and immunostained as described above. Graphs on the right from the images show the fluorescence intensity profiles analyzed in a longitudinal section (indicated by the yellow line) through focal adhesion. (C) The bar graph shows the percentage of focal adhesions enriched in presence of indicated GFP-ARHGAP42 variant. (D) The bar graph shows statistical analysis of relative enrichment of indicated GFP-ARHGAP42 variants in longitudinal sections through focal adhesions. The relative enrichment was calculated as a ratio of length given by the presence of GFP signal in a longitudinal section through focal adhesion (as shown in B)) and length of the focal adhesion (defined by the P-paxillin signal). Only focal adhesions positive to GFP-ARHGAP42 signal were analyzed. (C, D) Numbers in the histogram bars indicate number of focal adhesions analyzed. Error bars represent standard errors. Statistical significances were determined by one-way ANOVA followed by Tukey's post-hoc test.

Supplemental Figure S3.

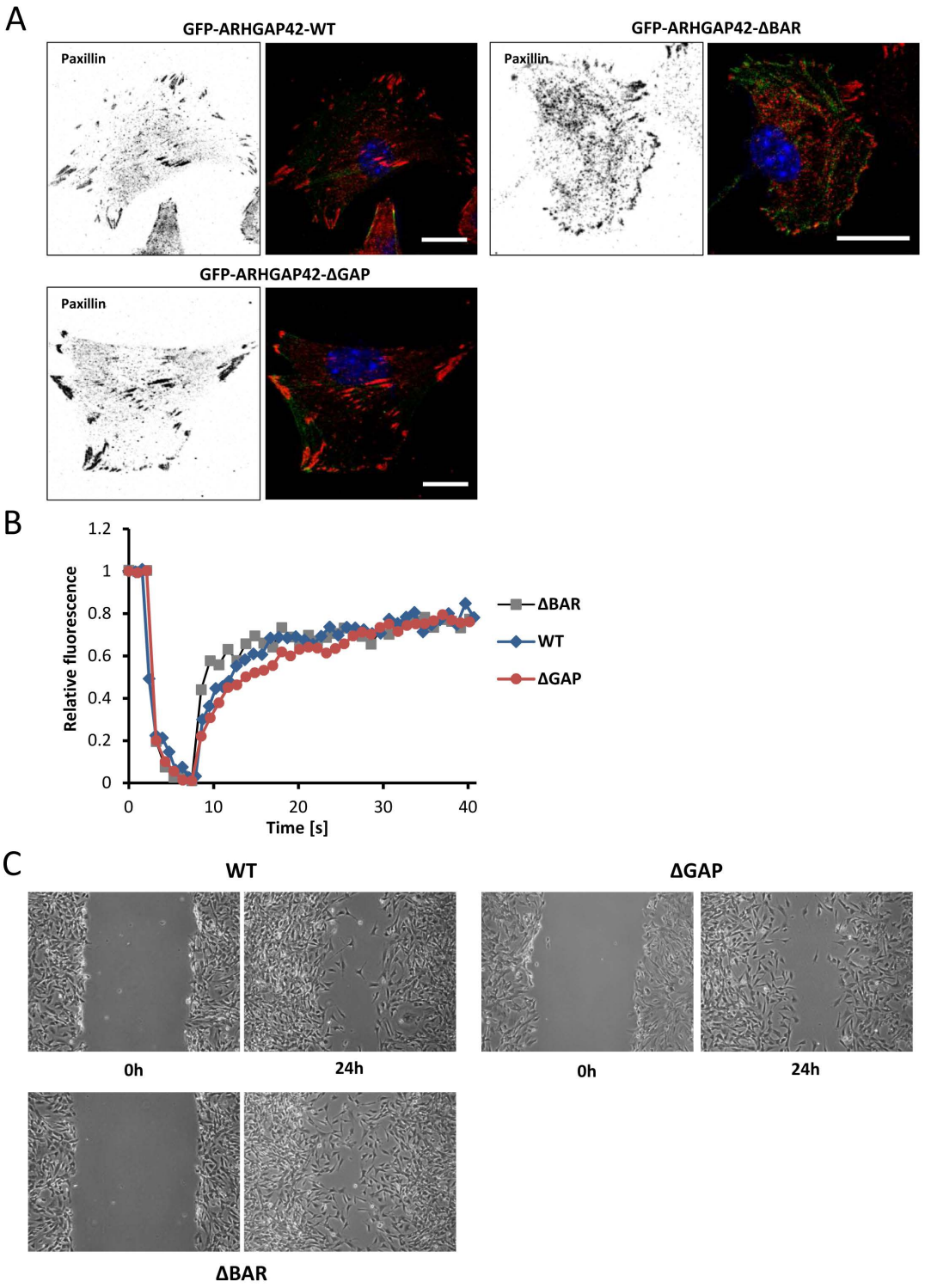

Supplemental Figure S3. Expression of ARHGAP42-ΔGAP increases the size of focal adhesions. MEFs stably expressing GFP-ARHGAP42 variants (WT, ΔBAR, ΔGAP) were grown on fibronectin-coated cover slips, fixed and focal adhesion size was analyzed by fluorescence microscopy. The cells were immunostained with an antibody against paxillin to mark focal adhesions. (A) Representative images showing focal adhesions stained by paxillin; left: greyscale signal of paxillin, right: merge (blue: DAPI, green: GFP, red: Paxillin). Scale bars are 20 µm. (B) Representative FRAP curves of mCherry-Vinculin dynamics in focal adhesions in MEFs expressing indicated variants of ARHGAP42. (C) Representative images of monolayer wound healing of MEFs expressing GFP-ARHGAP42 variants WT, ΔBAR, and ΔGAP.

Supplemental Figure S4.

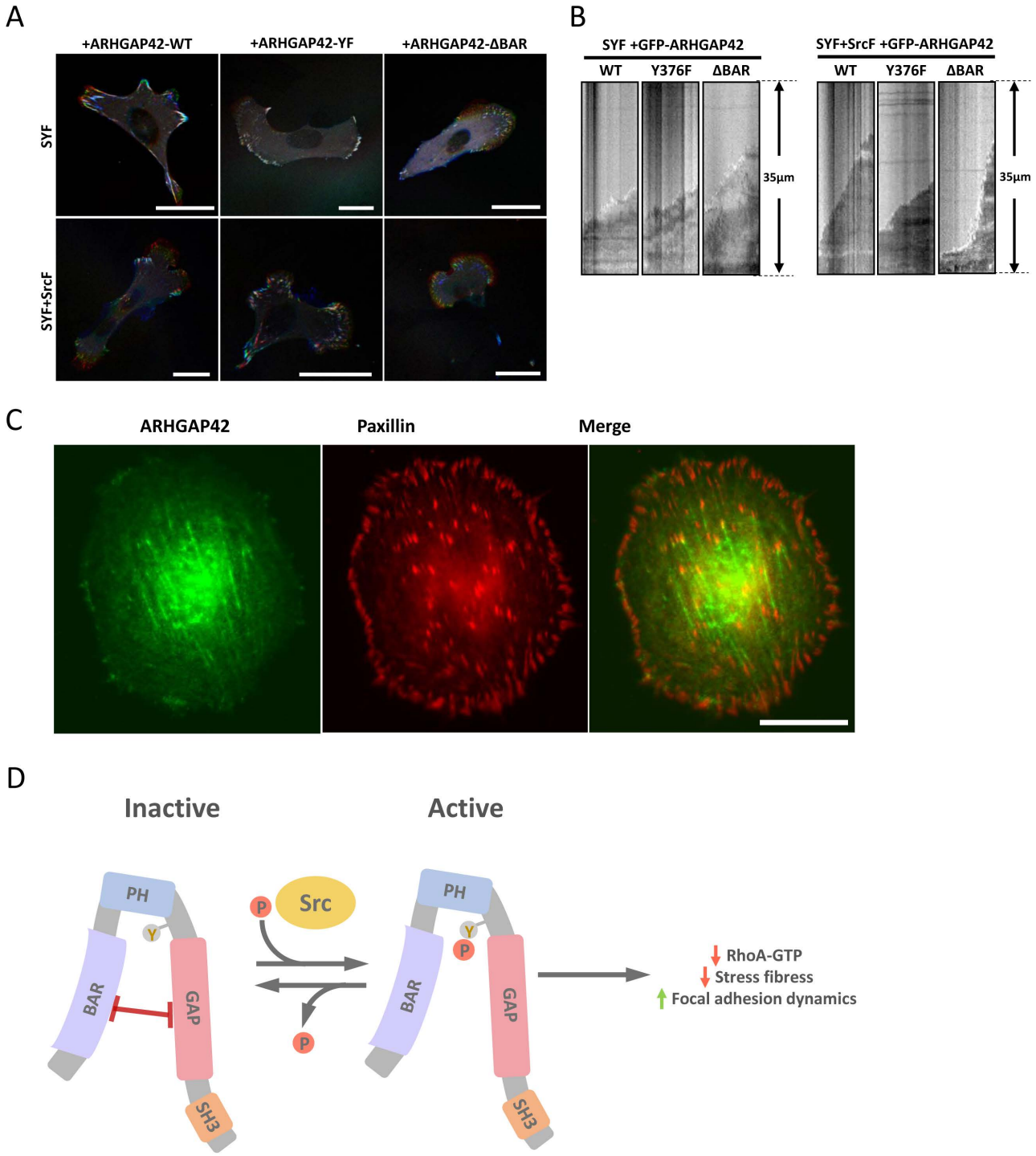

Supplemental Figure S4. (A, B) Src phosphorylation of ARHGAP42 on Tyr376 regulates focal adhesion and lamellipodial dynamics. SYF cells or SYF cells expressing constitutively active Src (SrcF) were co-transfected with GFP-ARHGAP42 expression plasmids (WT, Y376F, and ΔBAR). Cells were plated on fibronectin covered glass bottom dishes and after 24 hours cells showing similar levels of GFP-ARHGAP42 fluorescence, judged using an integrated intensity value of the GFP signal per cell and acquired with same settings (exposure, laser power, detector gain, etc.) of the microscope, were analyzed by confocal live cell microscopy. (A) Representative color-coded images of cell expressing ARHGAP42 variants observed for 10 min. Color coding: 0 min – blue, 5 min – green, 10 min – red; dynamic adhesions are colored and stable adhesions are white. (B) Representative kymographs of protruding lamellipodia showing increased lamellipodium velocity in cells with increased ARHGAP42 activity. **(C) Subcellular localization of endogenous ARHGAP42.** MEFs were immunostained with ARHGAP42 antibody (green, endogenous ARHGAP42) and anti-Paxillin (red) antibody to mark focal adhesions. Scale bars is 30 µm. **(D) Model showing ARHGAP42 activation by Src.** The BAR and GAP domains are inhibitory towards one another. Upon Src phosphorylation of Tyr-376 the inhibition is disrupted. Activation of the GAP domain leads to a decrease of RhoA-GTP levels and subsequently to lowering of acto-myosin tension, increased focal adhesion dynamics and loss of stress fibers.